78-4901

BESSEY, John Stewart, 1949-
PICOSECOND SPECTROPHYSICS OF SEMICONDUCTORS

The University of Arizona, Ph.D., 1977
Physics, solid state

University Microfilms International, Ann Arbor, Michigan 48106

PICOSECOND SPECTROPHYSICS OF SEMICONDUCTORS

by

John Stewart Bessey

A Dissertation Submitted to the Faculty of the

DEPARTMENT OF PHYSICS

In Partial Fulfillment of the Requirements
For the Degree of

DOCTOR OF PHILOSOPHY

In the Graduate College

THE UNIVERSITY OF ARIZONA

1 9 7 7

THE UNIVERSITY OF ARIZONA

GRADUATE COLLEGE

I hereby recommend that this dissertation prepared under my direction by John Stewart Bessey

entitled Picosecond Spectrophysics of Semiconductors

be accepted as fulfilling the dissertation requirement for the degree of Doctor of Philosophy

M Scully 11/14/77

Dissertation Director Date

As members of the Final Examination Committee, we certify that we have read this dissertation and agree that it may be presented for final defense.

R. Shanley	11/4/77
Ray Emrich	11/14/77
M. Scully	11/14/77

Final approval and acceptance of this dissertation is contingent on the candidate's adequate performance and defense thereof at the final oral examination.

STATEMENT BY AUTHOR

This dissertation has been submitted in partial fulfillment of requirements for an advanced degree at The University of Arizona and is deposited in the University Library to be made available to borrowers under rules of the Library.

Brief quotations from this dissertation are allowable without special permission, provided that accurate acknowledgment of source is made. Requests for permission for extended quotation from or reproduction of this manuscript in whole or in part may be granted by the head of the major department or the Dean of the Graduate College when in his judgment the proposed use of the material is in the interests of scholarship. In all other instances, however, permission must be obtained from the author.

SIGNED: John Stewart Bessey

To the Graduate College--

"Long May It Waive"

ACKNOWLEDGMENTS

I wish to acknowledge the support--scholastic, social, and financial--of the people with whom I have been in contact during my university years. I especially wish to thank the following people:

Ed and Sue Middlesworth, Pierre and Beate Meystre, and Eric van Stryland have provided a combination of professional and social friendship that would be hard to match.

Steve Barwick, Steve Harris, and Bob Schweiker have been the best of roommates and friends.

Hank van Driel, Art Smirl, and Bruno Bosacchi have been of incalculable help in my growth as a scientist and researcher. The best parts of what follows are the results of their guidance.

Molly Hennessy, Kay Bergsten, Phyllis Miller, and Martha Stockton have graciously tolerated my handwriting, my writing style, and my indecision in typing papers, letters, and this dissertation.

Fred Hopf, Rick Shoemaker, T. W. Nee, and John McCullen have been inspirations, both scientific and academic.

Marlan Scully has been that and much more: counselor, advisor, moneyman, guru, and friend. In the future may his life be blessed with students better than I.

I must also acknowledge, above all other contributions, the faith, friendship, and support of my parents, without which I would not be where I am now.

TABLE OF CONTENTS

TABLE OF CONTENTS--Continued

LIST OF ILLUSTRATIONS

LIST OF ILLUSTRATIONS--Continued

LIST OF TABLES

ABSTRACT

Solid-state physics is being revolutionized by the application of ultrashort optical pulse techniques to classical problems in such fields as hot electron plasma studies. In the work presented here, optical pulses of several picoseconds duration have been used to observe the ultrafast transient response of hot electron-hole plasmas in optically excited germanium, extending the approach of previous researches in the field to new experimental configurations. By considering the effects of varying temperature, pressure, and incident intensity in conjunction with studies of a series of germanium films of different thicknesses, we have attempted to lay a quantitative groundwork for future research into fundamental electronic processes in solids.

CHAPTER 1

INTRODUCTION

The introduction of the mode-locked Nd:glass laser has provided researchers with an optical tool capable of producing high-intensity, ultrashort optical pulses. Its pulselength ($\sim$5-10 psec) is on the same or shorter time scale as many of the processes that are important to the electron-hole plasma dynamics of semiconductors. This results in a powerful capability for use of the glass laser in excitation and observation of phenomena that were outside the range of sources available in the recent past.

With the setup and operation of a single-stage mode-locked Nd:glass laser oscillator at the Optical Sciences Center, The University of Arizona, a long-term program was begin to delve in detail into the transient response of optically excited electron-hole plasmas in a wide range of semiconductors covering a wide range of phenomena. The pioneering experiments by Smirl[1] and Matter,[2] coupled with those of other groups (most notably Auston and Shank at Bell Labs),[3] opened up a whole new field of endeavor. This eventually led to the mammoth theoretical paper on ultrafast carrier relaxation in germanium by Elci, Scully, Smirl, and Matter[4] (hereafter referred to as ESSM), closing out the first generation of experiments.

In this manuscript we hope to provide the reader with insight on the second generation experiments, utilizing as a basis the technology and theoretical background built up in the prior effort. The range of phenomena directly considered experimentally are more varied in both the timescales involved and the techniques applied, as we attempt to further the experimental and theoretical base underlying the processes in which we are interested.

A number of opportunities thus present themselves. The primary experiments performed were as follows, with goals of the experiments outlined briefly here.

Pressure Dependence of Single Pulse Transmission in Germanium

The band gap of germanium at room temperature can be tuned by application of hydrostatic pressure. This provides an opportunity to study the role of the band gap in various models of band filling by optically excited electrons. The results here are in excellent agreement with the model of ESSM.

Pulsewidth Dependence of Single Pulse Transmission in Germanium

ESSM predicts a variation in the transmission of ultrashort pulses in germanium depending on the duration of the incident pulses. Our experiment provides a suggestion that the model they propose is not complete,as our results are at odds with their predictions. We include here a discussion of the experimental results.

Radiative Recombination in Germanium

We present here a development from first principles of the theory of spontaneous photoluminescence in germanium. Experiments we carried out along these lines provide the impetus for a discussion of the feasibility of achieving significant stimulated emission and conceivably laser action in intrinsic germanium samples.

Optical Characteristics of Ultrathin Ge Films as a Function of Film Thickness

Our studies of the Ge laser concept suggested using ultrathin Ge films as an active medium. In preparation for this work we obtained several vapor phase epitaxially grown films (thickness 0.5 μm to 8 μm). These are initially studied by considering the same range of experiments performed by Smirl and Matter on mechanically polished films. The results presented here are compared to the predictions of the model of ESSM.

Putting everything into perspective at this early stage, we believe we have provided a significant input to the extension of the techniques and theory of previous workers in the field and have also provided justification for furthering the effort both theoretically and experimentally, in particular with respect to relaxing some of the assumptions originally made in the model proposed by ESSM.

CHAPTER 2

ULTRASHORT PROCESSES

We will first delve into experiments involving processes that are essentially over in the length of the incident mode-locked pulse, i.e., up to a maximum on the order of 15 psec. These are primarily concerned with excitation and heating of the carrier distribution and are studied by observing the transmission of optical pulses while the crystal sample is subjected to a series of external perturbations. The original experiments of Smirl and Matter involved study of the transmission of single pulses as a function of incident energy at 1.06 μm at two sample temperatures. Their data (105 K data are shown in Fig. 1) show an increase in transmission above Beer's law absorption as the coupled states in the conduction (valence) band become filled with electrons (holes) as a result of the intense excitation. This reduces the number of available valence band electron-conduction band hole pairs that can absorb photons. The model used to explain these data is given in ESSM. From that paper it is apparent that two experiments would be of immediate interest for comparison to the model. These are studies of the saturation of transmission of ultrashort pulses as functions of (1) the relative energies of the semiconductor band gap and the incident photons and (2) the pulsewidth of the incident radiation.

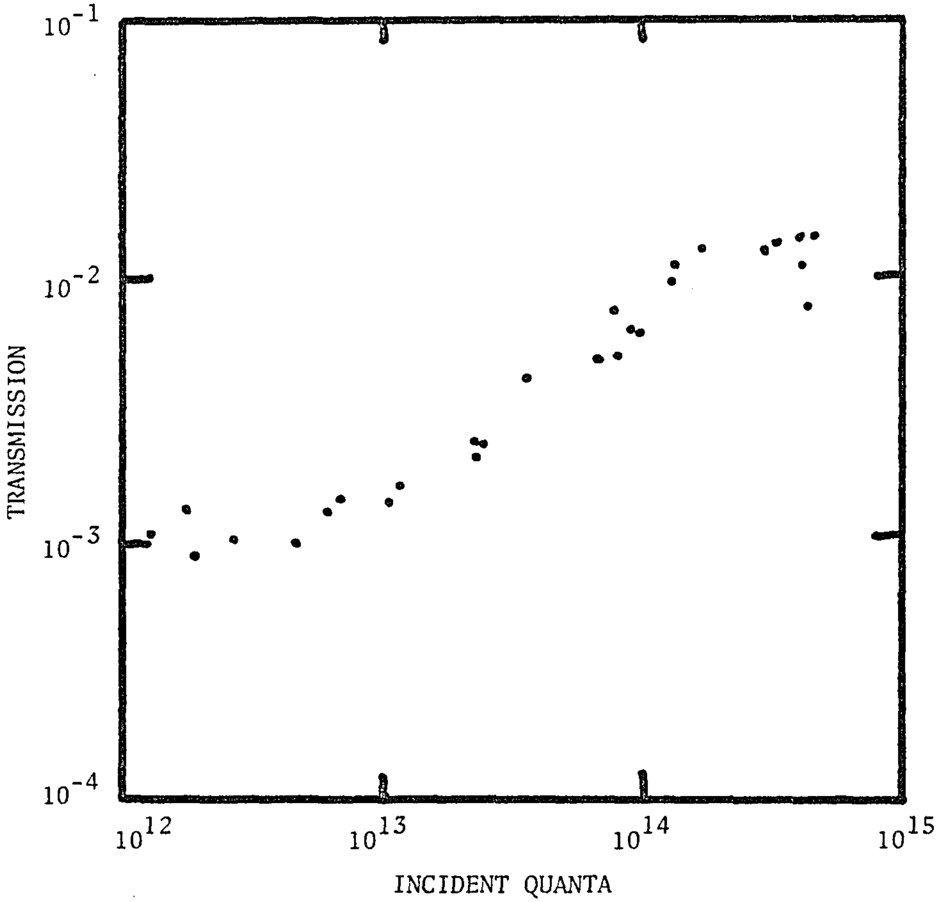

Fig. 1. Transmission of Ultrashort Pulses as a Function of Pulse Energy for a 5.2-μm-Thick Sample at a Temperature of 105 K (from ESSM).

There are a number of alternatives for the first. We may take a whole series of semiconductors of different gaps with one laser or a tunable high power ultrashort pulse laser with one semiconductor. Unfortunately the semiconductor and laser situations are both rather restricted as there are neither sufficient numbers of suitable semiconductors nor any high power tunable picosecond lasers. However, a compromise can be reached, as will be seen in the next section, by varying the band gap in germanium by application of hydrostatic pressure. The results are in basic agreement with ESSM.

The second series of experiments is rather easier to perform but has had wider repercussions with the model advanced by ESSM. The pulsewidth experiments have been in general disagreement with ESSM at the high intensity end of the transmission curves. Adjustments to the theory of ESSM to account for these differences have been studied[5] and are outlined briefly here.

In addition another series of experiments was carried out. All of the work to date on Ge, especially with respect to the model of ESSM, has been carried out on samples of thickness $\sim 5\ \mu m$. It was determined that several points of the theory could be brought into better focus by considering a wide range of sample thicknesses. We obtained several thicknesses of vapor phase epitaxially grown Ge films on GaAs substrate which we have studied to determine the effects of decreasing thickness on such important processes as diffusion of the excited carriers.

Pressure Tuning of Picosecond Pulse Transmission in Germanium

The development of the gasketed diamond anvil pressure cell[6] has given the world a source of hydrostatic pressure upwards of 100 kbar for small sample volumes. This easily exceeds the 30+ kbar needed to increase the room temperature band gap of germanium above the laser photon energy (see Fig. 2). Thus the direct band gap can be tuned continuously from the atmospheric pressure T=295 K value of .805 eV to above the laser photon energy, at which point the sample becomes essentially transparent to the incident pulses. This provides a method of studying the electron band filling associated with ultrashort pulse excitation.

The diamond anvil cell, shown in Fig. 3, obtains high pressure by applying opposite forces to a pair of ¼ carat diamonds whose culets have been ground and polished to ∿0.75 mm across. Between the diamonds is a beryllium-copper washer with a 0.5-mm-diameter hole drilled in the center. The active cell volume uses a 4:1 mixture of methyl-ethyl alcohol as an incompressible fluid, in which floats a small ruby chip and the semiconductor sample. The measurement of the shift of the ruby doublet fluorescence from 6942Å ($\Delta\lambda$ = 0.365 Å/kbar)[7] provides absolute pressure determination to ±1 kbar.

The experimental apparatus is shown in Fig. 4. The incident laser pulses are focused onto the germanium sample,which is a high purity (ρ_{min} = 40.0 ohm•cm) single crystal of thickness 5.2 μm and covers approximately one-half of the open-cell aperture. The focused spot size with a 20 cm focal length lens is about 200 μm diameter. The

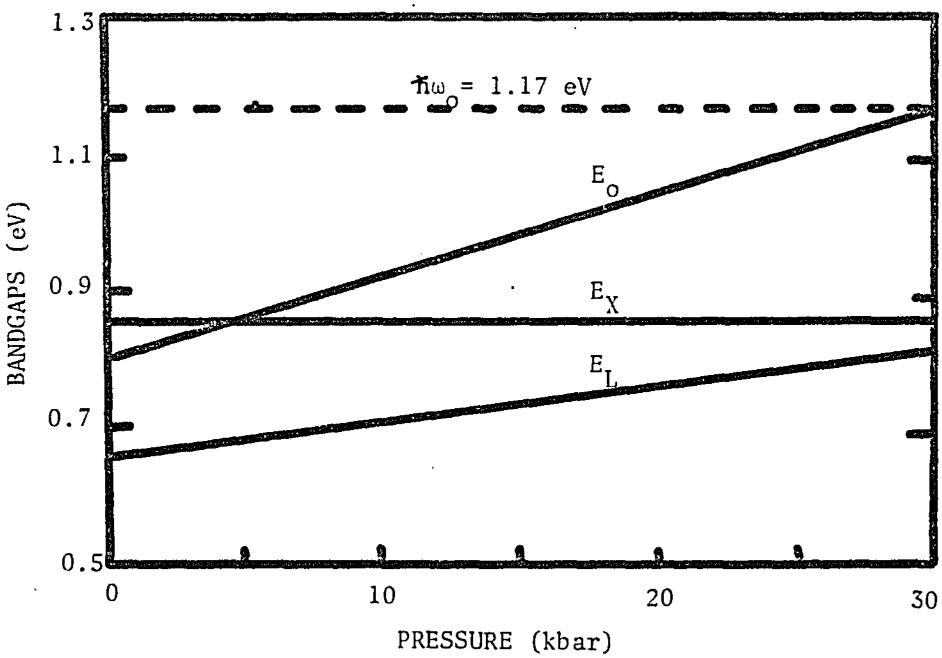

Fig. 2. Pressure Dependence of the Band Gaps in Germanium at T = 295 K.

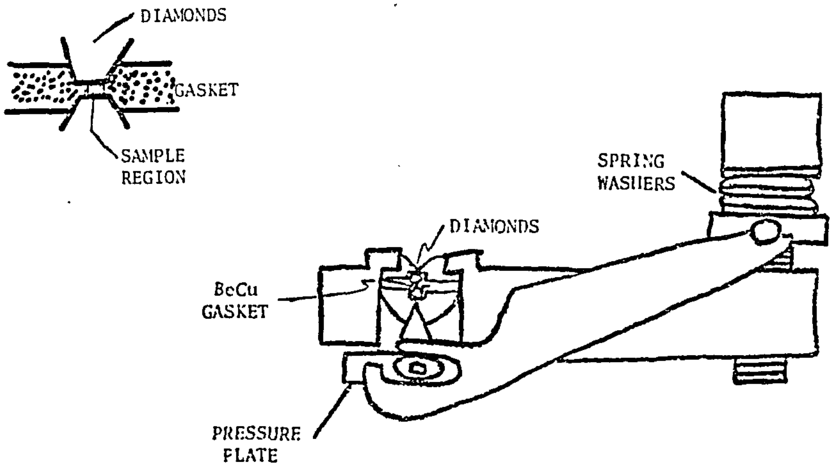

Fig. 3. Schematic of the Diamond Anvil Pressure Cell Developed by Piermarini.[6]

Inset shows an enlargement of the sample cell region.

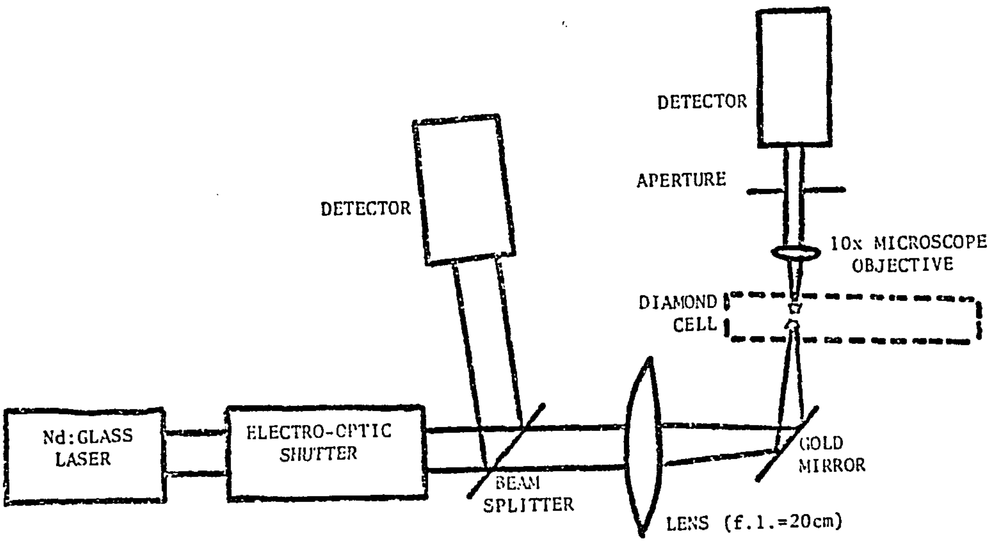

Fig. 4. Diagram of Pressure Experiment Apparatus.

sample was imaged onto the apertured face of the detectors following the technique described by Welber,[8] thus allowing us to significantly reduce the amount of stray light getting into the detector system. The absolute determination of the transmissivities was carried out by performing measurements both on and off the sample inside the cell so that the transmission reference level accounted for absorptions and reflections that were unrelated to the phenomena that we wished to study. This was accomplished by positioning the cell with an X-Y translation stage.

The experimental result of transmission as a function of incident pulse intensity is shown in Fig. 5 for pressures up to 24 kbar. All data are corrected for sample reflectivity and cell transmission. The data at 1 bar are from Smirl et al.,[9] obtained with an equivalent sample at a temperature of 295 K outside the pressure cell, and are included here for comparison. The lower limit of pulse intensity is determined by detector sensitivity while the upper limit is determined by the damage threshhold of the sample. At the highest pressure shown (24 kbar), the direct band gap has been increased to 1.09 eV ($dE_o/dP \sim 12\times10^{-3}$eV/kbar)[10] compared to the laser photon energy of 1.17 eV. Overall, the data show an enhanced transparency at high pulse intensities which increases from a factor of three at 1 bar to a factor of ten at 9 kbar. The transparency enhancement then decreases steadily to a step of 50% at 24 kbar.

These data can be clearly interpreted within the model of ESSM where several processes, whose rates (γ) are comparable to or

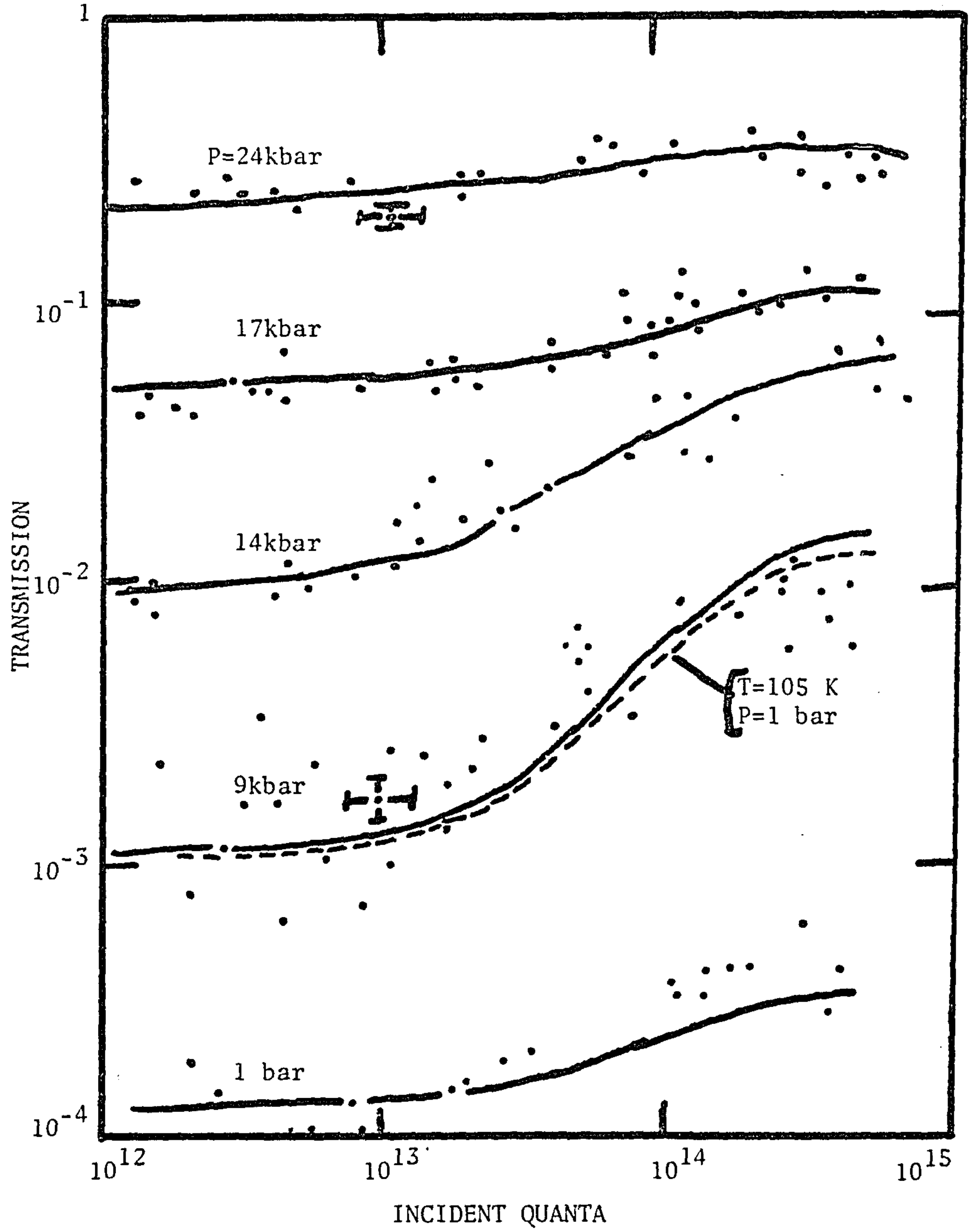

Fig. 5. Transmission of Ultrashort Pulses as a Function of Pulse Energy for Different Sample Pressures at 295 K.

Solid lines indicate fit of the model of ESSM to the data. Dashed line is a theoretical curve for T = 105 K and P = 1 bar.

faster than the inverse pulse width, determine the transmission. Direct absorption ($\gamma_{DA} \sim 10^{14}$/s) creates the electron-hole plasma with electrons being scattered ($\gamma_S \sim 10^{14}$/s) between the Brillouin zone center valley (Γ) and boundary valleys (L,X). Coulomb thermalization through carrier-carrier interactions ($\gamma_{c-c} \sim 10^{10}$/s) which elevates optically excited carriers to even higher energy states serves to heat the carrier distribution. Once the density of carriers is sufficiently high ($>10^{19}/cm^3$) that the plasmon energy is comparable to the direct gap, electrons and holes are able to recombine with the creation of plasmons. The density of carriers (n) is therefore being reduced at a rate

$$\frac{dn}{dt} = -k(n_\Gamma - \bar{n}_\Gamma) \tag{2.1}$$

where k is a constant and $\bar{n}_\Gamma$ and n_Γ are equilibrium and nonequilibrium densities of electrons in the Γ conduction band valley. Because the plasmon resonance is considerably broadened by fluctuations in the Fermi levels while the pulse is on, the plasmons return their energy to the individual carriers in a time short compared to the pulse width ($\gamma_{PAR} \sim 10^{+14}$/s). This plasmon-assisted recombination process dramatically heats the carrier distribution ($T_{plasma} > 10^3$ K), thereby drastically reducing the occupancy of the optically coupled states.

The effect of pressure on each of the above processes is as follows. The direct absorption coefficient in the Beer's law region will decrease with increasing pressure, reflecting a decrease in the joint density of states for $\hbar\omega = 1.17$ eV as the valence and conduction bands move apart. The carrier-carrier interaction is independent of pressure as is the free carrier absorption process if one makes the reasonable assumption that the electron-phonon interaction does not change significantly with pressure. The last process that has to be considered, plasmon-assisted recombination, should display a significant pressure dependence. Because the PAR process occurs when the density of carriers is such that the plasmon energy becomes comparable to the direct gap energy, an increase in the direct band gap with pressure should lead to a decrease in the efficiency of the PAR process. This would result in a decreased plasma temperature for a given pulse energy. A more subtle secondary effect in the reduction of the PAR rate occurs because the indirect energy gaps do not increase as fast ($dE_X/dP \sim 0$, $dE_L/dP = 5 \times 10^{-3}$ eV/kbar)[11] as the direct gap with increasing pressure. Therefore, all other effects being equal, the ratio of Γ valley to L,X valley electrons--and therefore the PAR rate--decreases with increasing pressure.

Incorporating the above processes using the known physical parameters of germanium, transmission curves for the appropriate pressures were generated and are shown by the solid lines in Fig. 5. The agreement of the model with the data is quite remarkable and provides convincing evidence that the model is intrinsically correct. Indeed, any discrepancy between theory and experiment is most likely due to the omission of spatial effects, e.g., pulse propagation in the model.

Within the context of the model, the increase and then decrease in enhanced transparency with increasing pressure occur because of a decrease in the PAR rate, plasma temperature, and Γ valley electron density. On increasing the pressure from 1 bar, the dominant effect is a reduced PAR rate that allows for a denser but slightly cooler plasma.

This results in the optically coupled electron-hole states becoming more occupied than at the lower pressure and therefore allowing a higher transmission. This trend continues up to a pressure of $\sim$10 kbar as predicted by the model and verified experimentally. Beyond this pressure the increasing separation of the Γ and L,X conduction band valleys becomes felt as the Γ valley receives less than its previous share of electrons. This, together with the decreasing plasma temperature, allows the tail of the Fermi distribution to move down in the Γ valley, opening up the coupled electron states, thereby reducing the nonlinear transmission.

It becomes interesting to compare the results presented here with the earlier work of Smirl et al.,[9] who measured the nonlinear transmission of germanium at 295 K and 105 K. At 105 K the band gaps of germanium are approximately the same as they are at 10 kbar and 295 K. The order of magnitude increase in the transparency of germanium at 105 K is also about the same as we observe at 9 kbar. Indeed, the theoretical prediction for the transmissivity as a function of pulse energy at 105 K is shown by the dashed line in Fig. 5 and is close to the behavior exhibited by the 9 kbar data. This result allows us to draw two conclusions. First, the temperature-dependent (through phonons) free carrier absorption process is not important in heating the optically generated plasma and influencing the nonlinear transmission. Second, the earlier work of Smirl et al., which displayed a temperature dependence of the nonlinear absorption, did so only because of the accompanying changes in the direct band gap, with similar results being obtainable by pure volume effects alone.

Pulsewidth Dependence of Nonlinear Transmission of Picosecond Pulses in Germanium

As was seen in the last section, the initial experiments on a picosecond time scale produced excellent agreement with the theory of ESSM. An interesting feature of the model presented by ESSM is the predicted strong dependence of the nonlinear transmission of intense ultrashort optical pulses through germanium on the width of the optical pulses. This pulsewidth dependence is depicted in Fig. 6, which is taken from ESSM. This figure represents the theoretical transmission of a 5.2-μm-thick sample of germanium as a function of the number of incident quanta at $\lambda_L = 1.06$ μm for a sample temperature of 77 K and for theoretical optical pulses of widths of 2.5, 5, and 10 psec.

The pulsewidth dependence of the transmission can be understood in terms of this model in the following way.[12] Initially, when the optical pulse enters the Ge sample, most of it is absorbed, creating a large number of electrons (holes) in the central valley of the conduction (valence) band. These electrons are rapidly (compared to a picosecond) scattered to the conduction band side valleys by phonons. Carrier-carrier scattering events ensure that the carrier distribution is Fermi-like. Since the laser photon energy $\hbar\omega_o$ is greater than the direct band gap E_o and the indirect band gap E_G, a direct absorption event such as the one just described gives an excess energy of approximagely $\hbar\omega_o - E_G$ to electronic thermal agitation. Thus, these processes result in a large number of electrons (holes) in the conduction (valence) band at a relatively high carrier temperature (T_e is approximately 1500 K; refer to ESSM). If only these processes are

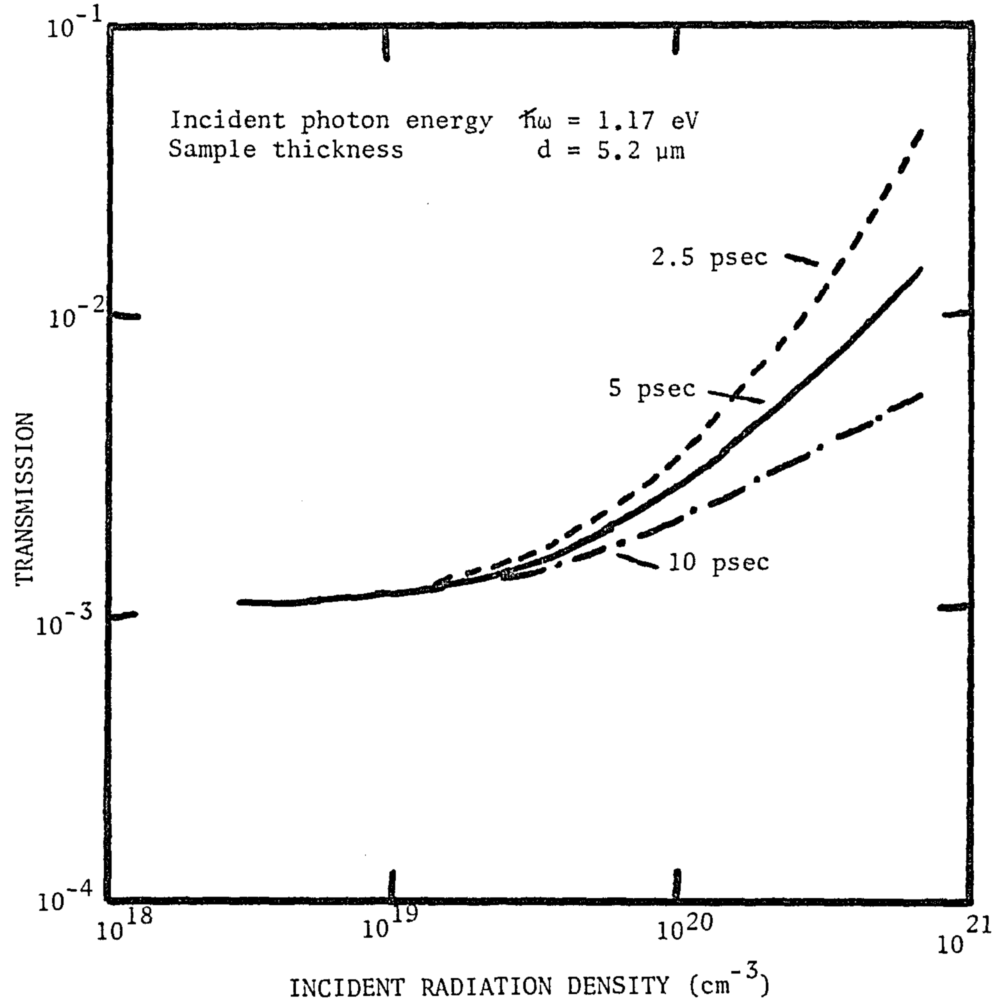

Fig. 6. Theoretical Prediction of Transmission of Ultrashort Pulses as a Function of Pulse Energy for Incident Pulsewidths of 2.5, 5, and 10 psec (from ESSM).

considered, the Ge transmission will rise as the optical pulse energy is increased, owing to the saturation of the available optically coupled states, but no dependence on pulsewidth will result. However, intra-valley electron-phonon relaxation and plasmon-assisted electron-hole recombination, when included, will cool or heat, respectively, the carrier distribution. If the phonon-assisted cooling dominates, more of the electrons (holes) will be located lower (higher) in the conduction (valence) band, thus more completely filling the states needed for absorption; the transmission will further increase. However, if heating due to plasmon-assisted recombination is the stronger, the electrons (holes) will be located higher (lower) in the conduction (valence) band, thus freeing the states needed for optical absorption; the transmission will increase more slowly as a function of optical pulse energy. To understand the pulsewidth dependence of these two processes, consider two pulses of equal energy but different width incident on a Ge sample. While the longer pulse interacts with the sample there is more time for both phonon-assisted relaxation and plasmon-assisted recombination. If heating due to plasmon emission is dominant, the longer pulse will have the higher distribution temperature, and, consequently, the lower transmission. If the phonon-assisted relaxation is stronger, similar arguments show the transmission will have the opposite pulse width dependence. Although we have simplified the situation somewhat, these are the dominant effects. The coupling constants in the ESSM paper were such that phonon-assisted cooling of the carrier distribution was small during the time the pulse was present in the sample; thus plasmon heating effects determined the pulsewidth dependence.

A schematic of the experimental apparatus used to make these measurements is shown in Fig. 7. A single pulse of width τ of 5-10 psec is switched from the train of pulses from the laser. To produce variable-width pulses, this single optical pulse is split into two separate parts, which are then recombined collinearly after one part has been delayed with respect to the other with a Michelson interferometer. The recombined pulse is then focused on the sample to a spot with diameter of approximately 250 μm. The sample is undoped, high purity (ρ_{min} = 40.0 ohm·cm), single-crystal germanium with the (111) plane as the face, mounted on a KZF-2 substrate and polished to a thickness of 7.5 μm, as determined by an interferometric technique.

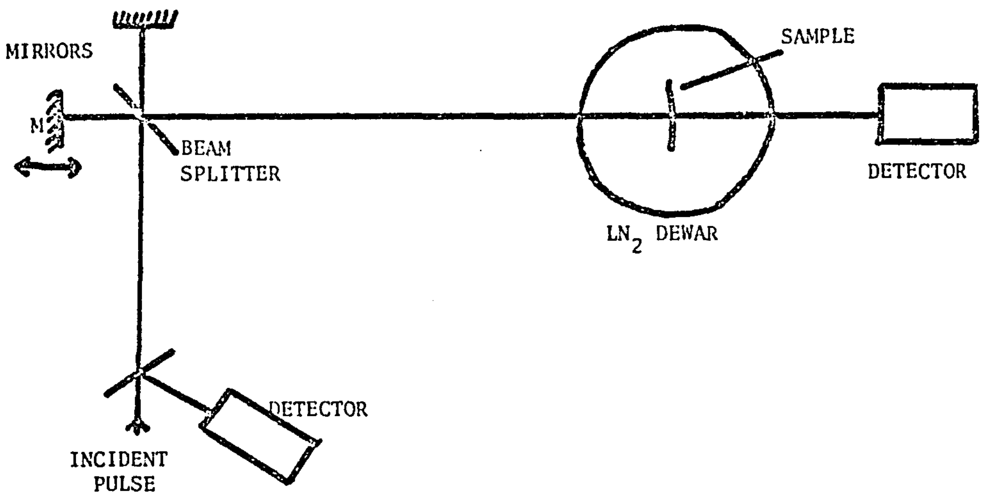

Fig. 7. Schematic Diagram of Variable Pulsewidth Apparatus.

The pulsewidth is varied by moving the mirror M to change the path length of one arm of the interferometer.

Figure 8 is a plot of the transmission versus incident pulse energy for two pulsewidths, τ ($\sim$8 psec) and 2τ, for a sample temperature of 105 K. Each point shown is the average of 8 to 12 data points, and the error bars represent one standard deviation. It is readily seen that the difference between the two curves is less than the uncertainties in the data and substantially less than predicted by theory.

Thus we are left with the first substantial discrepancy between experimental results and the model proposed by ESSM. Recent work by Smirl et al.[5] has shown that some of these discrepancies may be toned down by varying the electron-phonon and electron-plasmon coupling constants for germanium.

Thickness Study of Germanium Films

Two of the fundamental assumptions of the model proposed by ESSM are homogeneous excitation of the sample and a subsequent diffusionless dynamics of the excited carriers. The ellipsometry experiments of Shank and Auston[13] at Bell Laboratories have shown that in at least some cases diffusion is significant, and the validity of this assumption is currently being studied theoretically at The University of Arizona. The assumption of homogeneous excitation is at low energies a simplifying one at best, as the 1/e length for Beer's law absorption of 1.17 eV photons in germanium is on the order of 1 μm.

To date little has been done with the specific intent of directly studying these assumptions on an experimental basis for thin ($\lesssim$10 μm) samples. This is specifically due to the extremely important problems that arise in the usual method of preparing thin germanium

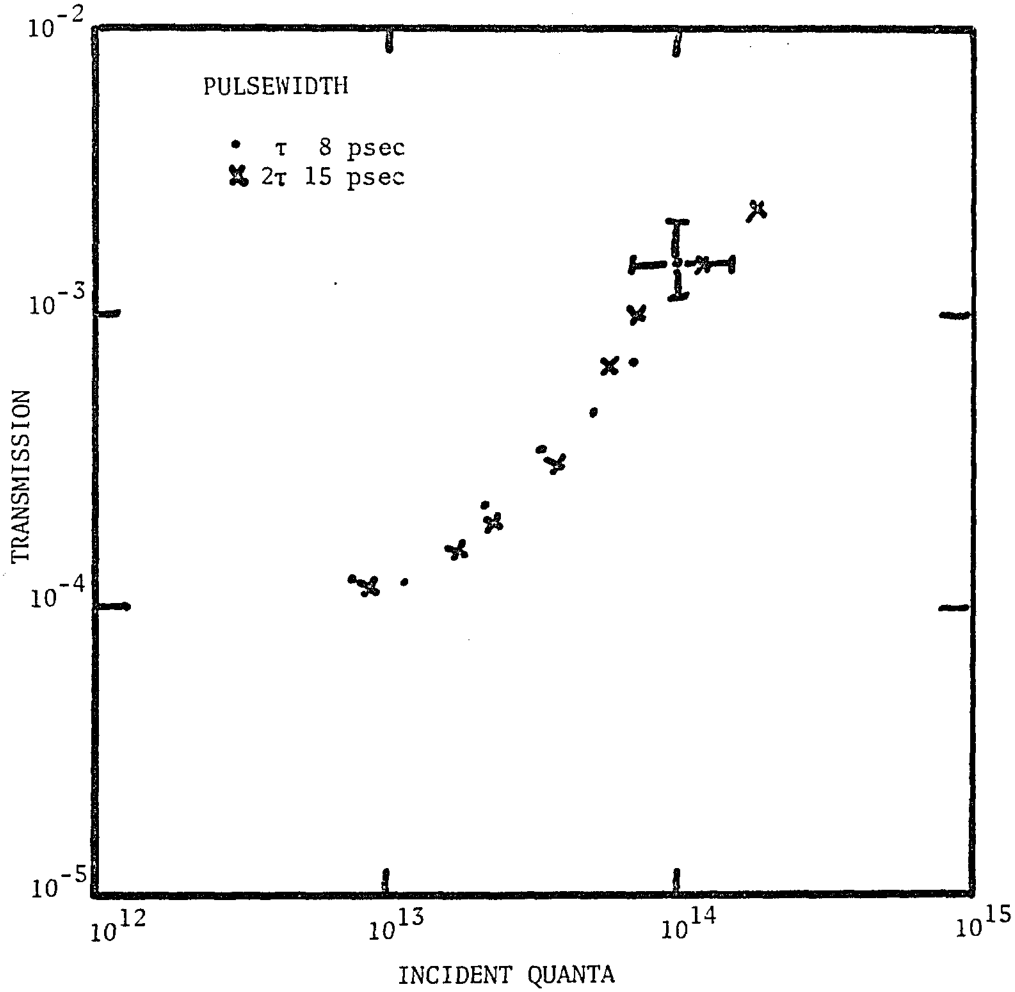

Fig. 8. Transmission of Ultrashort Pulses as a Function of Pulse Energy for Incident Pulsewidths τ and 2τ.

samples. A piece of bulk single-crystal intrinsic germanium that has been mechanically polished and chemically etched on one face is epoxied to a substrate of KZF-2 glass, providing a firm base that has nearly the same thermal expansion coefficient as the germanium. The mounted sample is then polished and etched to produce a Ge film that is several micrometers thick with parallel faces. This is limited to producing samples on the order of 5 μm. Thus the experiments to date have been performed on samples of thickness 5 to 8 μm.

In addition to these mechanical problems, two other related problems arise. These are the directly coupled problems of cost of manufacture (nearly $1000 per sample) and a dearth of optical technicians with the equipment and experience to produce high-quality samples. Thus an experimental program to seriously study the previously mentioned aspects of excitation and diffusion would require an excessive amount of funding just for samples that would not span the sample thickness range required to pin down these effects. With this in mind we have undertaken such an experimental program, with one fundamental difference: the samples we are using are produced by vapor phase epitaxial deposition on gallium arsenide substrates. The major difficulties inherent in the mechanical polishing process--thickness and cost--are not problems for the VPE-grown samples, as the apparatus that produces the samples, after the initial setup costs, can be run for little more than the cost of materials. Any thickness desired can be achieved by varying the growth rates and times. Of course there are problems that are uniquely associated with such samples. The atom-by-atom growth that occurs, in order to form a single crystal structure, must be forced into the desired crystalline configuration. GaAs has been chosen as a substrate to provide a close match to the lattice constant and structure of the Ge that will be laid down. The relatively good match between Ge and GaAs does not guarantee that the Ge will be single-crystalline, but electron diffraction tests on our samples have shown that the Ge films are in general good-quality single-crystal samples of homogeneous thickness. The major drawback to the samples we have used is that the surfaces are not all of an extremely high visual quality. The exact effect this has on our results is yet to be determined. The heterojunction character of the transition region between the Ge and the GaAs is another major unknown. Since this region is on the order of 100 Å thick, it is most likely negligible in the experiments we have undertaken. This transition region warrants further study. In addition, two-photon absorption (TPA) of the glass laser photons occurs in the GaAs. We have ignored this effect for our samples, as peak transmissions of the thinnest Ge films are around a few percent, so the energy incident on the substrate will be below the point where significant TPA will occur. For thinner samples this effect must be taken into account.

The Ge samples we used ranged in thickness from 2.6 to 6.8 μm, on GaAs substrates of ∿100-200 μm. Characteristics of the samples are given in Table I. The Ge thicknesses were calculated from the Beer's law absorption region of the 1.0-μm single-pulse transmission curves assuming the low-intensity absorption coefficients given by ESSM.[4]

Our experiments follow along the lines of those originally performed by Smirl[1] and Matter.[2] These include single-pulse transmission as a function of incident pulse energy and transmission of a weak probe

Table I. Characteristics of VPE-Grown Germanium Films.

Sample	Thickness (μm)	Quality
M25T	6.8	Good
M28B	3.5	Good
M31B	3.1	Fair
80B	2.6	Poor

pulse as a function of time delay after an intense excitation pulse. Both have been carried out on all samples at temperatures of 295 K and 105 K, the latter achieved by mounting the sample on the cold finger of a small liquid nitrogen dewar. A schematic diagram of the experimental setup is shown in Fig. 9, and the probe delay apparatus is detailed in Fig. 10. The pulse energy is monitored by detector D_1, providing a shot-to-shot calibration of the energy incident on the sample. The pulse is then split into two parts by the beamsplitter B, and each part is reflected off a right-angle Porro prism P and gold-coated front-surface mirror M. One of the Porro prisms is mounted on a micrometer stage, allowing one to dial in any desired delay over a range of approximately 150 psec (3-mm motion of the micrometer stage corresponds to 20-psec delay). For the excitation-probe experiment, the probe beam is attenuated by a 4% transmission dielectric filter and the two beams are then focused onto the sample. This achieves a 25:1 excitation-to-probe pulse energy ratio, ensuring that the excitation pulse is well into the saturated region of the single pulse transmission spectrum while the probe pulse is in the Beer's law transmission region. Thus the probe pulse will be a minor perturbation on the excited carrier plasma and will thus

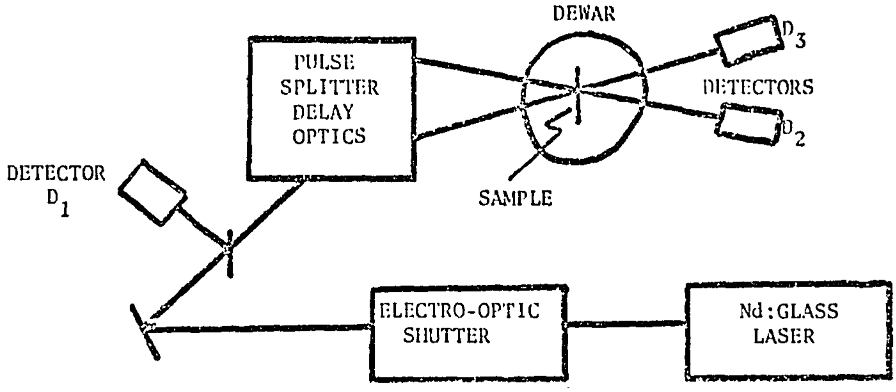

Fig. 9. Apparatus for Pulse-Probe Experiments.

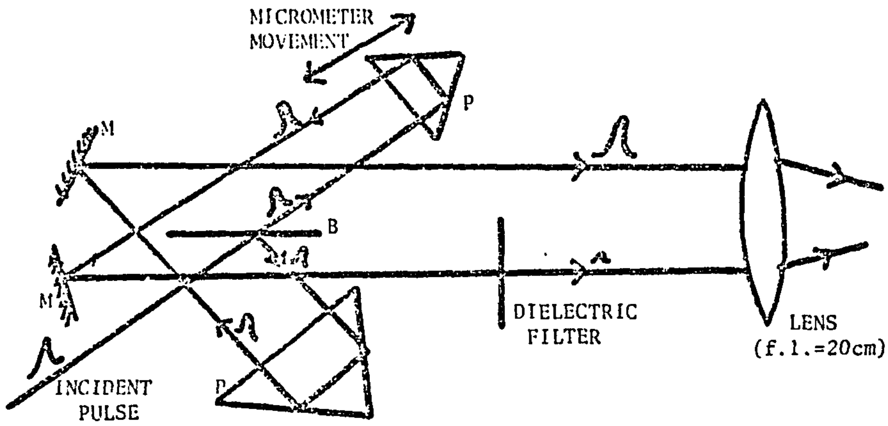

Fig. 10. Details of Pulse Splitter-Delay Optics.

provide information on the state of the evolving plasma. The beams are focused to a spot diameter of about 250 μm and carefully overlapped on the sample. The transmitted beams are focused into the detectors D_2 and D_3, which measure the transmitted energy. A 1.06-μm laser line filter is placed after the sample to block any photoluminescence from the two-photon absorption excited GaAs substrate.

Single-Pulse Transmission Experiment

The single-pulse transmission data are taken by blocking the probe pulse channel in the delay optics and varying the excitation channel energy with a series of interference filters. Figures 11 through 14 show the absolute sample transmission as a function of incident pulse energy for each sample at temperatures of 295 K and 105 K. These curves show the typical behavior reported in ESSM. The transmission begins low at small incident intensities as Beer's law absorption dominates. At higher intensities, the transmission begins to rise, owing to the decreasing number of available valence band electron-conduction band hole pairs that can be coupled by the incident radiation. At yet higher intensities, an extremely fast nonradiative recombination of the excited carriers begins to dominate, so the electrons are recycled down to the valence band as fast as they are excited into the conduction band. Thus the supply of valence band electrons is continuously replenished. The transmission peaks and in some cases begins to decrease. The latter effect occurs just below the damage threshold of the sample surface, which provides a limit to the incident intensity that one can couple into the sample and still maintain a meaningful experiment.

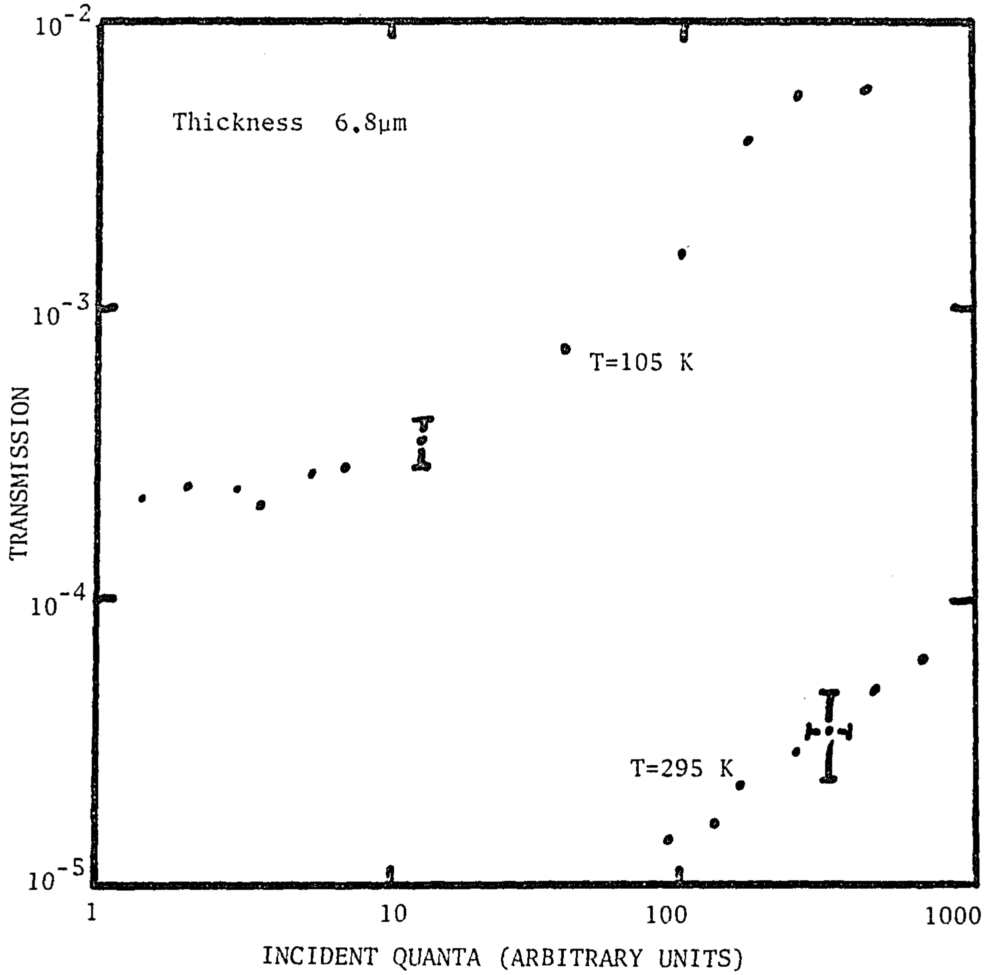

Fig. 11. Transmission of Sample M25T vs. Incident Pulse Energy.

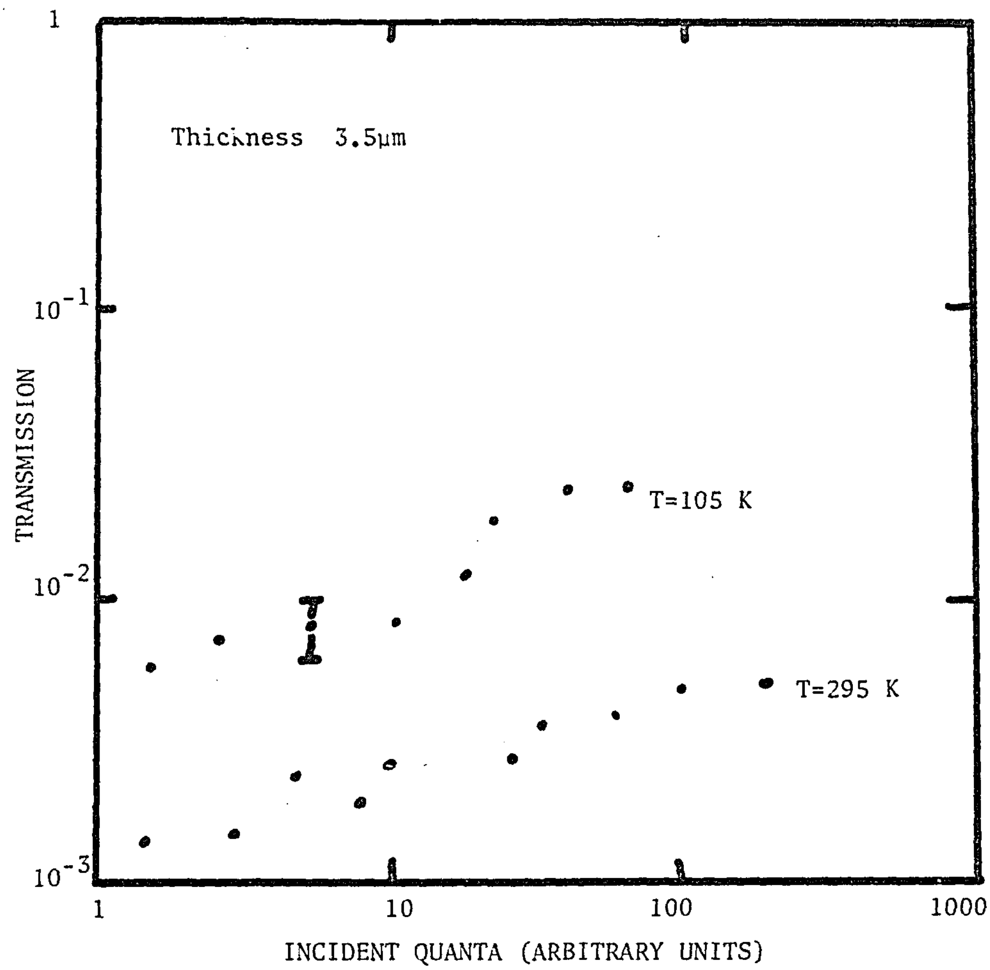

Fig. 12. Transmission of Sample M28B vs. Incident Pulse Energy.

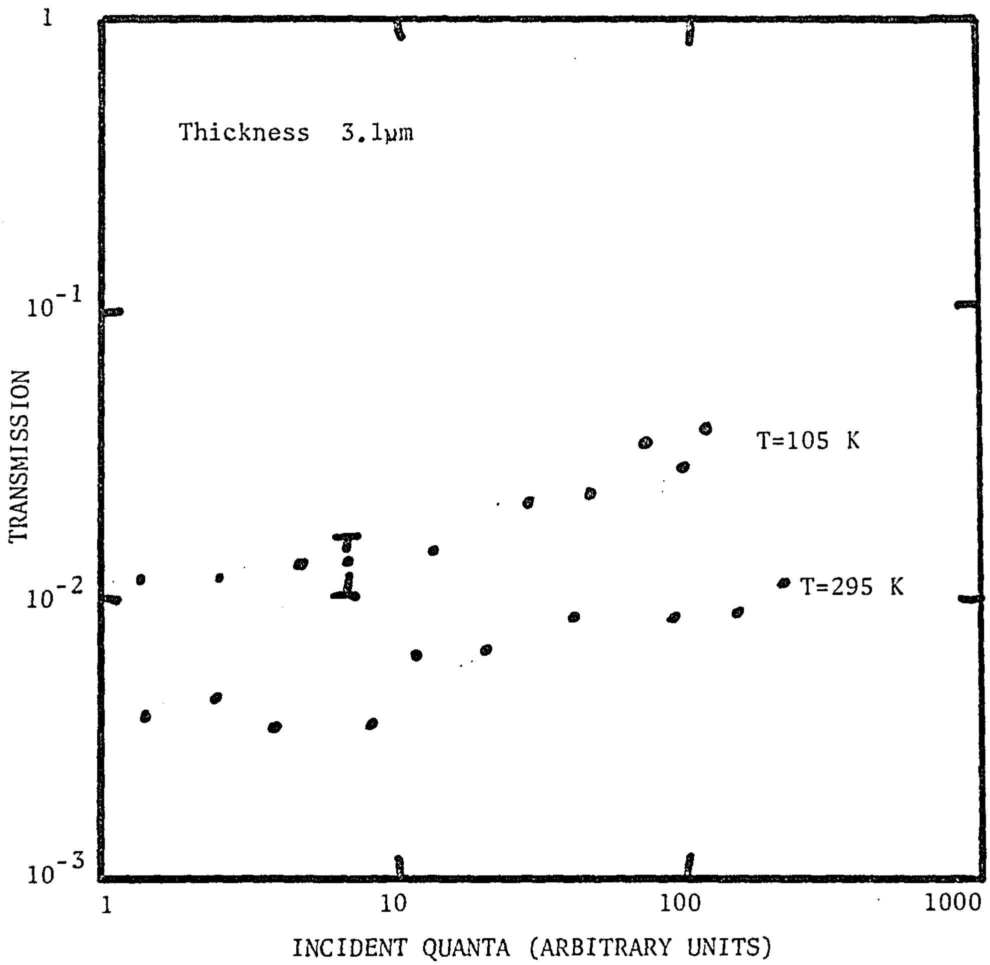

Fig. 13. Transmission of Sample M31B vs. Incident Pulse Energy.

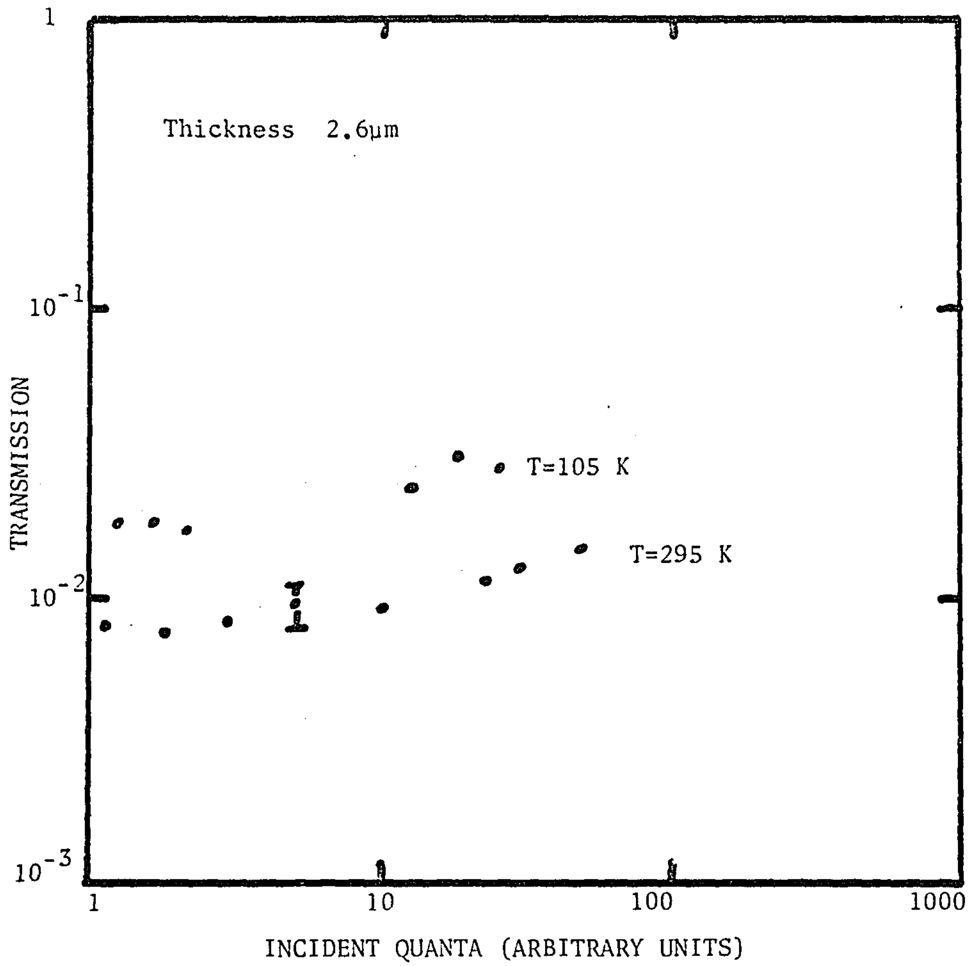

Fig. 14. Transmission of Sample 80B vs. Incident Pulse Energy.

The absorption coefficients in the Beer's law region are calculated by ESSM to be 1.48 μm^{-1} at 295 K and 1.10 μm^{-1} at 105 K. If we assume that the samples are uniformly excited and calculate an average absorption coefficient for each sample as a function of pulse energy, we obtain the curves in Figs. 15 and 16 for 295 K and 105 K, respectively. Except for the thick sample data at 295 K, all follow essentially the same general trends: the absorption coefficients start to fall (transmissions start to increase) at the same incident pulse energy, and they fall at approximately the same rate. As it is clear at the lowest incident energies that the excitation is not homogeneous, this trend suggests that it is not homogeneous at higher energies either. The saturation begins to occur in the front portions of the sample first, while the back portions remain in the Beer's law region. The reason for the peaking of the saturation is as follows: the higher incident energies cause a dramatic increase in the temperature and density of the excited carrier distribution in the front portion of the sample until the absorption process is so strong that only a fixed amount of energy is allowed through the front portion to saturate the back portion. Thus with the highest incident energies so much energy is pumped into the front portion of the sample that it is destroyed, producing the spot seen when the surface has been damaged by too high an incident energy.

Excitation-Probe Experiment

The probe pulse transmission for each sample is plotted as a function of time delay after the initial excitation pulse in Figs. 17 and 18 for T = 295 K and 105 K, respectively. All the curves have been

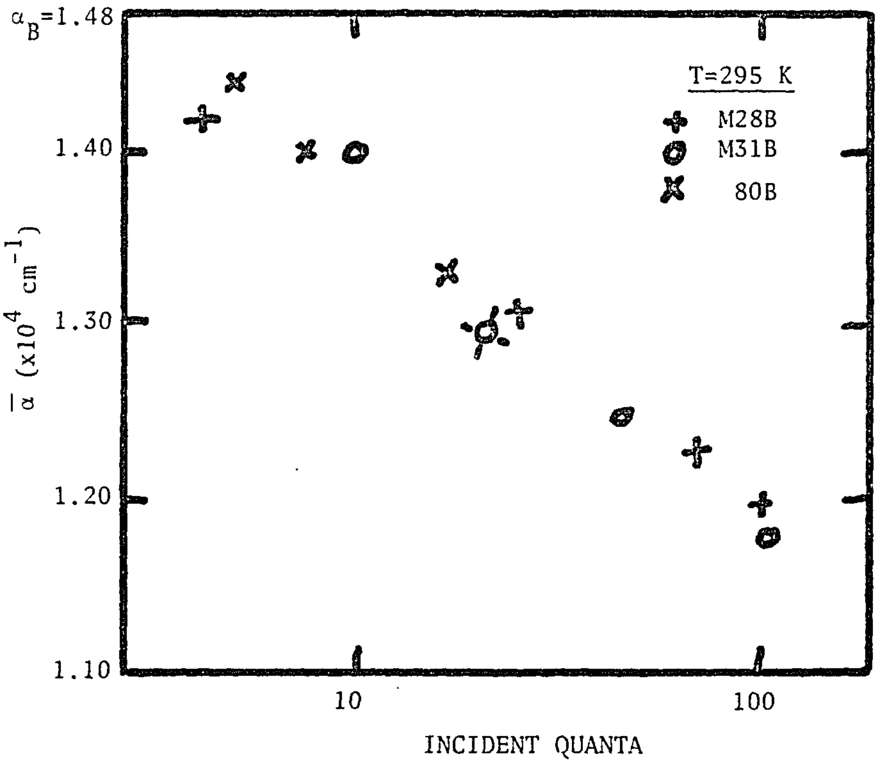

Fig. 15. Average Absorption Constant vs. Incident Pulse Energy at T = 295 K.

α_B is the Beer's law absorption coefficient calculated by ESSM.[1]

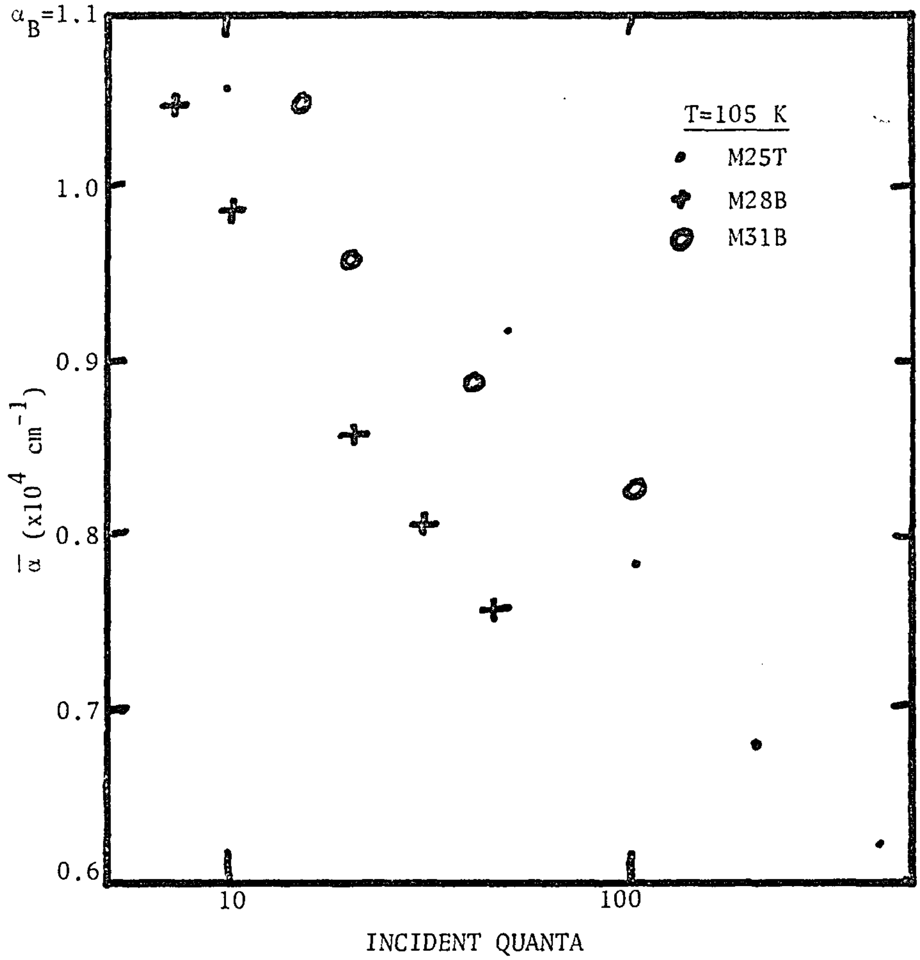

Fig. 16. Average Absorption Constant vs. Incident Pulse Energy at T = 105 K.

α_B is the Beer's law absorption coefficient calculated by ESSM.[1]

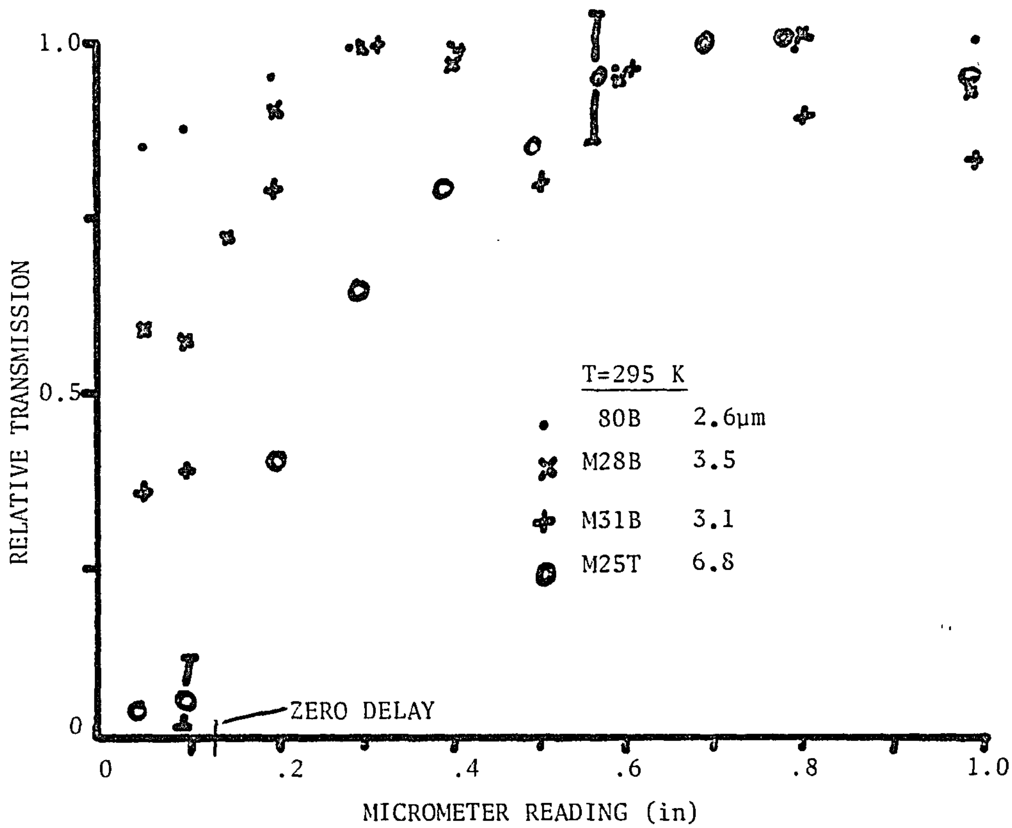

Fig. 17. Relative Probe Transmission vs. Probe Pulse Delay at T = 295 K.

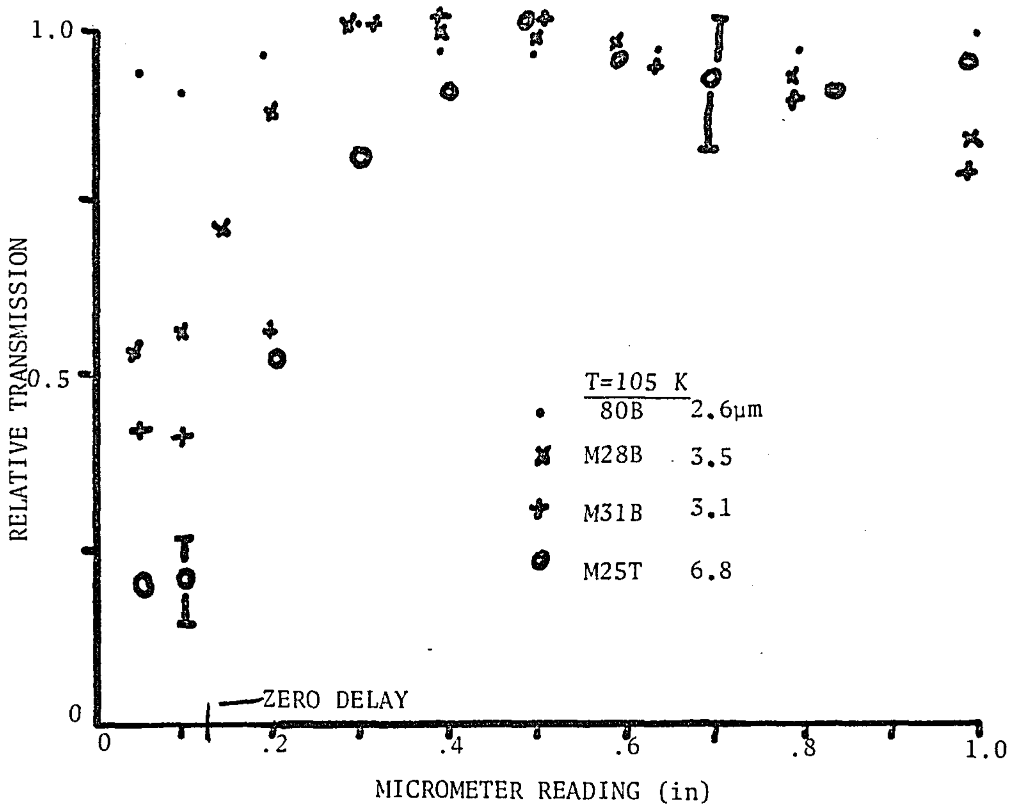

Fig. 18. Relative Probe Transmission vs. Probe Pulse Delay at T = 105 K.

normalized to the same peak value. As the two exhibit the same types of features, we shall concentrate on the T = 105 K curve for a qualitative description of the results. A number of features are of interest: (1) The initial (negative delay) transmissions show marked variations, (2) the transmission curves rise at slightly different rates and peak at different probe pulse delays; and (3) the curves appear to decay at almost the same rates. We shall discuss each of these points in turn.

The initial relative transmissions of the probe pulses are expected to be different. The ratio of the peak probe transmission to its undelayed transmission should be a measure of the ratio of the saturated excitation pulse transmission to the Beer's law transmission. As has been shown, the transmission enhancement decreases markedly with decreasing thickness. Thus the initial relative transmission for the thinner samples should be higher than for the thicker samples. This is borne out in general by Fig. 18.

One of the interesting points apparent from Fig. 18 is that the probe pulse transmission peaks at a shorter delay for the thinner samples than for the thicker ones. This can be explained by considering the diffusion of the excited hot carriers. In a thin sample, the carriers are excited nearly homogeneously across the sample, and diffusion is not significant. The probe pulse sees a highly excited sample at all times, so the rise time to the peak of the probe pulse transmission is dependent primarily on the relaxation of the excited carriers within the conduction band, filling up the absorption-coupled states. For thick samples, the front portions of the sample are initially highly excited, leading to a high probe transmission; but the later portions are not highly excited, so the probe pulse is initially strongly absorbed. In the first hundred picoseconds after the excitation, the dominant process affecting the probe pulse transmission is the diffusion of hot carriers into the less excited regions of the sample. The overall probe transmission increases because the increase in transmission through the portions of the sample that the carriers are diffusing into is greater than the decrease of the transmission through the early portions of the sample where the diffusion is causing a decrease in carrier density.

After the probe transmission peaks, it begins to decay at a rate that is essentially independent of sample thickness. This is expected, as further carrier relaxation should depend on intensive features of the sample such as band structure and interparticle coupling constants rather than on extensive features such as film thickness. This also supports the previously stated belief that the films are of generally even crystalline quality.

The end result of these experiments is to call into question the two assumptions of ESSM mentioned previously, i.e., homogeneous excitation and diffusionless carrier dynamics. But these experiments do not provide definitive proof, as there are numerous details to be considered. For example, the lattice mismatch between the Ge and the GaAs produces a large unilateral strain in the Ge layer.[14]

CHAPTER 3

PHOTOLUMINESCENCE IN GERMANIUM

We now turn to a second time scale in optically excited germanium. In Chapter 2 we were interested in processes occurring as we pass a large pulse of light through the sample. As the pulses are on the order of 8 psec long, any process taking longer than 1 nsec is of no consequence to the observations. In this chapter we turn our viewpoint completely around. Instead of monitoring the excitation pulse after it has passed through the sample, we blast away at the sample and then do everything we can to avoid seeing the incident pulse at all. Instead we are interested in the slower processes that occur in the sample, monitored by observation of the luminescence given off by the sample during the time when the excited carriers are relaxing back to their equilibrium conditions. We first historically review the initial attempts to observe radiative recombination in germanium. After a discussion of the relevant properties of this semiconductor, we provide a "first-principles" approach to the theory of photoluminescence in germanium including diffusion effects. This is then compared with a series of experimental observations. In summary we then discuss the probability for achieving direct gap lasing in this indirect gap material.

Historical Background

Over the past several years there have been considerable interest and much success in inducing laser action in semiconductors, primarily centered on the development of sources in the infrared. However, one group of materials in which experiments along these lines have been entirely unsuccessful is the indirect gap semiconductors. It is generally accepted that attempts to bridge the indirect gap with phonon assisted transitions will not result in useful stimulated emission, as the loss due to absorption by free carriers is considerably higher than the gain across the indirect gap.[15] However, calculations by Adams and Landsberg[16] have shown direct gap laser action may be possible. In particular, they estimate that in an ideal case a conduction band electron population of $\sim 3\times10^{19}$ cm^{-3} could be sufficient for laser action across the direct gap in germanium. In the course of the study of the ultrashort transient response of excited carrier plasmas in germanium[1-4,9] it was determined that such densities, although very near the damage threshhold of the sample, could be readily obtained.

As a first step we consider spontaneous recombination radiation in optically excited germanium. Photoluminescence from germanium has been known for a quarter century, beginning with observations by Haynes and Briggs[17] and by Newman.[18] Calculations by Haynes and Nilsson[19] using a detailed balance argument predict an efficiency for direct radiative recombination a factor of 10^6 higher than for the indirect process. This would lead one to expect a direct photoluminescence that is significantly larger than the indirect photoluminescence. However, in nearly all reported observations to date, the overwhelming bulk of the radiation was due to recombination across the indirect gap. In only one case has more direct than indirect luminescence been seen,[19] in a thin ($\sim 7\ \mu m$) sample excited to low carrier densities by a mercury arc lamp and observed at the front surface, i.e., the surface toward the source of excitation.

To understand the failure of early observations to see direct radiation, we consider the typical experimental techniques. The continuous output from a thermal light source such as a tungsten lamp is passed through a water cell to block out the infrared component of the lamp spectrum and focused on the front surface of the sample. The radiation emitted from the opposite back surface of the sample is spectrally analyzed by a monochromator and a photodetector. Owing to the highly efficient absorption of the visible portion of the lamp spectral output by the sample, this signal radiation consists entirely of the germanium photoluminescence. Herein also lies the difficulty in the observation of the direct gap radiation. The incident radiation is absorbed in a layer on the sample surface a few micrometers thick. Any direct photoluminescence emitted by carrier recombination in this region has to traverse the entire thickness of the sample before reaching the monochromator. The processes that lead to the high direct recombination rate make the corresponding reabsorption rate equivalently high. This would not be a problem in a direct gap semiconductor, but in an indirect gap material like germanium it presents great difficulties, as in order to build up a substantial direct valley population, one must first nearly fill the indirect valleys. Except in the region near the front surface of the sample where the incident radiation is absorbed, the indirect valleys are nearly empty, and any electrons promoted to the conduction band by absorption of the direct gap photoluminescence would scatter into the side valleys before they could recombine again across the direct gap.

Recently, we reported observation[20] of significant direct gap photoluminescence in bulk intrinsic germanium. In these experiments the thick ($\sim$ 100-μm) sample was excited with optical pulses from a Nd:glass laser (λ = 1.06 μm) and the photoluminescence observed from the front surface using a novel mirror and sample arrangement. The direct photoluminescence must then travel less than a diffusion length ($\sim$ 20 μm) through the sample. Use of the Nd:glass laser has the additional advantage that high incident powers can be achieved, raising the effective electron Fermi level well into the conduction band. The tail of the electron distribution then reaches above the direct energy gap, ensuring that a significant number of electrons can recombine via the direct process. Our techniques therefore are favored over the traditional approach on the grounds of a more probable population of the central conduction valley and a superior method of observation of the emitted radiation.

Radiative Recombination: Band Model

Germanium Band Structure

Germanium is an indirect gap semiconductor[21,22] (Fig. 19) that crystallizes in a diamond-type lattice with two atoms per unit cell and

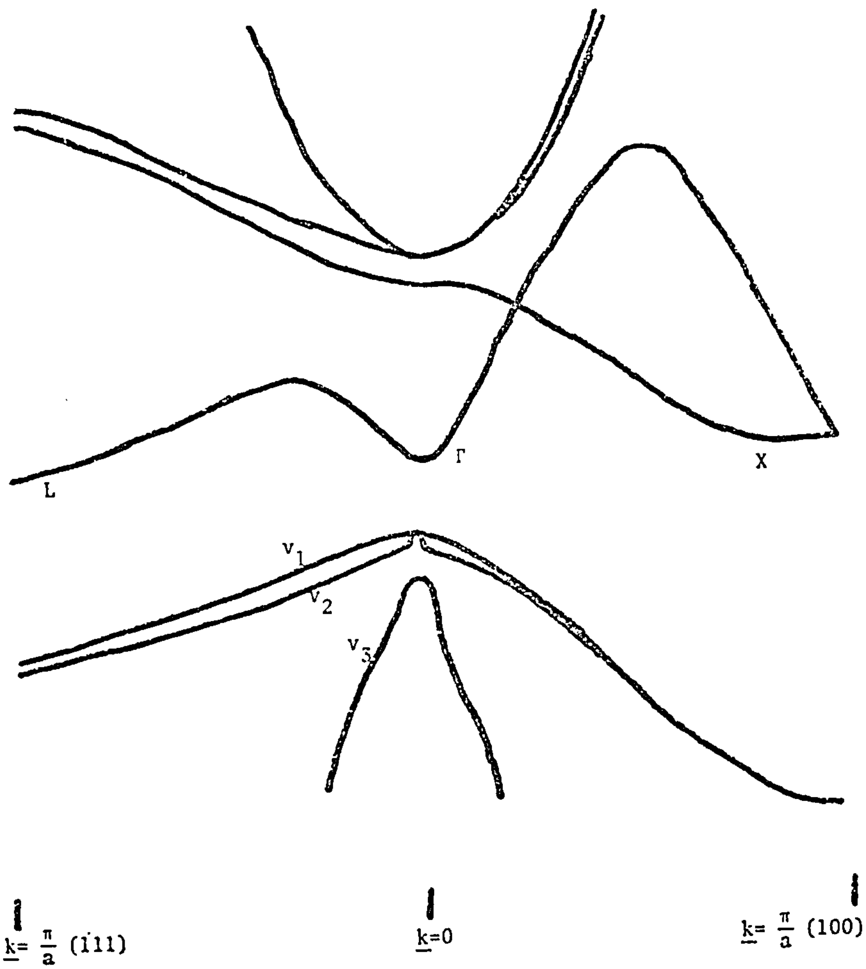

Fig. 19. Germanium Energy Band Structure.

lattice constant a $\sim$ 5.657 Å. The valence band consists of two nearly degenerate heavy hole bands v_1 and two light hole bands v_2 with another band v_3 split off .285 eV by spin-orbit coupling. The conduction band edge is at the L-point [(111) direction] of the Brillouin zone at a relative energy .664 eV above the valence band edge at room temperature. There are four equivalent L-point valleys in the conduction band. The direct gap at the Γ-point (zone center) is .805 eV at room temperature. There are also six X-point [(100) direction] valleys at a relative energy of .86 eV. The constant energy surfaces of all of the bands are ellipsoids with effective masses given in Table II. The relative positions of the split off hole band and the X-point conduction valleys and the small effective mass of the light hole bands will allow us to ignore these bands in the processes we will consider. We restrict our attention to the two heavy hole valence bands and the four L-point and one Γ-point conduction valleys.

The phonon-assisted processes of interest are between zone center and the vicinity of the L-point. Transverse-phonon-assisted electron transitions between the Γ valley and the L valleys are forbidden by symmetry considerations so we need only consider longitudinal acoustical and longitudinal optical phonons. The L-point phonon energies are 27 meV and 30 meV for LA and LO mode phonons, respectively.[22]

There are two radiative recombination processes of importance. The direct transition of an electron from the Γ conduction valley to the valence band is a first order process resulting in emission of a photon (see Fig. 20). Indirect transitions are second order, characterized

Table II. Band Parameters of Germanium.[22]

Band	Energy (eV) at 295 K	$\frac{dE}{dT}$ (meV/K)	Effective mass	Symbol
v_1	0.0		0.364	m_h
v_2	0.0		0.1	
v_3	-0.285			
Γ	0.805	-0.44	0.042	m_o
L	0.664	-0.37	0.22	m_c
X	0.805			

Masses are given in terms of the free electron mass, and the energies are of the band extreme relative to the valence band edge.

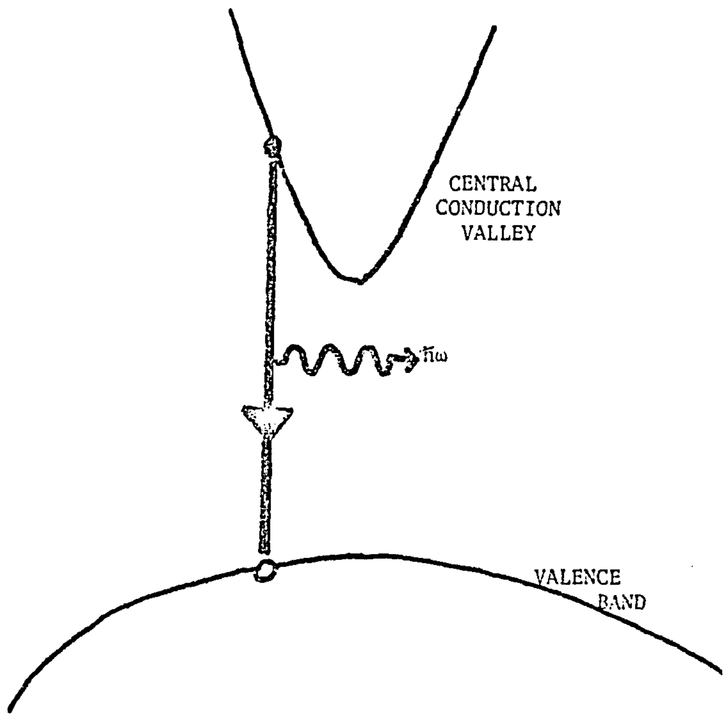

Fig. 20. Schematic Band Representation of Direct Recombination.

not only by the emission of a photon but also by interaction with a phonon. In one sequence (Fig. 21a) the electron of wavevector $\underline{k}$ goes to a virtual state of wavevector $\underline{k}$ in the valence band emitting a photon and then scatters to valence band wavevector $\underline{k} - \underline{q}$ by absorption or emission of a phonon of momentum $\underline{q}$. The other sequence (Fig. 21b) is a phonon-assisted transition from wavevector $\underline{k}$ in the L valley to a virtual state of wavevector $\underline{k} - \underline{q}$ in the Γ valley, followed by a direct transition to the valence band accompanied by emission of a photon.

As has been shown by a number of experiments[3,4] the relaxation of the electrons within the conduction band after the excitation of the sample occurs in a time on the order of 100 psec. The fastest radiative processes, direct recombinations, occur at a rate less than 10^9 sec^{-1} with the second order indirect processes a few orders of magnitude slower. Thus on a time scale much shorter than that of the processes in which we are interested, the electrons in the conduction band and the crystal phonon distribution can communicate with respect to temperature and wavevector distribution. Before the radiative processes become important, the electrons and holes will have achieved thermal equilibrium with the lattice at a temperature T, close to the initial lattice temperature. As a result, we shall make the excellent approximation that for all times of interest we can describe the conduction band electron and valence band hole distributions as Fermi-Dirac functions at the initial temperature T with Fermi quasi-levels E_F and E_H respectively. Denoting the energy of a particle in band i with wavevector $\underline{k}$ as $E_i(\underline{k})$, we then have the distributions ($\beta^{-1} = k_B T$ where k_B is Boltzmann's constant)

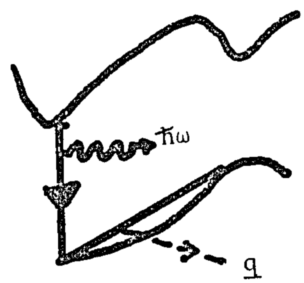

a.

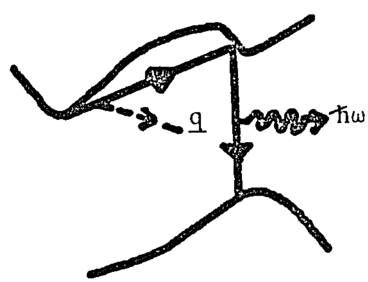

b.

Fig. 21. Schematic Band Representations of Indirect Recombination.

$$f_\Gamma(\underline{k}) = [1 + \exp \beta(E_\Gamma(\underline{k}) - E_F)]^{-1}$$

$$f_L(\underline{k}) = [1 + \exp \quad (E_L(\underline{k}) - E_F)]^{-1}$$

$$f_h(\underline{k}) = [1 + \exp \beta(E_h(\underline{k}) - E_H)]^{-1} \tag{3.1}$$

where we measure energies relative to the valence band edge. We have chosen to define the particle energies such that they are all positive and generally restrict ourselves to discussion of electrons only in the conduction band and holes only in the valence band.

We assume that, over the important portion of the bands, the particle energies may be described as quadratic functions of the wave-vector $\underline{k}$ with the appropriate effective masses. Thus the particle energies in the various bands are

$$E_\Gamma(\underline{k}) = E_o + \frac{\hbar^2}{2m_o} k^2$$

$$E_L(\underline{k}) = E_G + \frac{\hbar^2}{2m_c} (\underline{k} - \underline{k}_L)^2$$

$$E_h(\underline{k}) = \frac{\hbar^2}{2m_h} k^2 \tag{3.2}$$

where we measure $\underline{k}$ from the center of the Brillouin zone.

Direct Recombination

We consider the simpler direct recombination first. The processes that are important in determining the overall emitted radiation intensity concern electron transitions between the central conduction valley and the valence bands with emission of a photon. This is shown diagrammatically in Fig. 22. For completeness we include the absorption diagram to account for reabsorption of the emitted radiation. However,

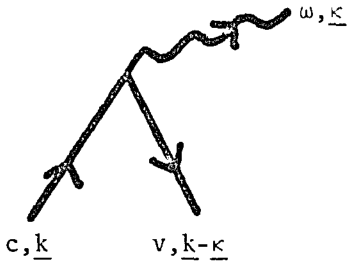

a.

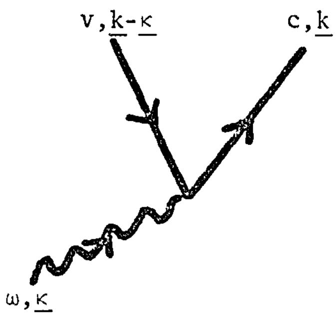

b.

Fig. 22. Direct Transitions Involving Emission or Absorption.

Emission (a) or absorption (b) of a photon (wavy lines) by electrons and holes (solid lines).

we shall in the final analysis consider absorption in a phenomenological manner only, as will be shown below. The absorption and emission processes are equivalent in their formalism. We describe the emission process below and then write out the equations involving both.

The probability per unit time of a transition is given by Fermi's Golden Rule

$$W_{fi} = \frac{2\pi}{\hbar} |M_{fi}|^2 \, \delta(E_f - E_i) \tag{3.3}$$

where M_{fi} is the matrix element of the interaction producing the transition between the initial (i) and final (f) states of the system. The δ-function ensures energy conservation. For the direct recombinations we are interested in the case where the initial state consists of N photons of frequency ω and wavevector $\kappa = \varepsilon_\infty^{\frac{1}{2}} \, \omega/c$, an electron in the Γ-valley of the conduction band with wavevector $\underline{k}$ and a hole in a valence band with wavevector $\underline{k} - \underline{\kappa}$. The interaction Hamiltonian is

$$H_{ep} = \frac{e}{mc} \underline{A} \cdot \underline{p} = \frac{e}{mc} \left(\frac{2\pi c^2 \hbar}{\varepsilon_\infty \omega} \right)^{\frac{1}{2}} (\hat{e}_\lambda \cdot \underline{p}) \; a_\kappa^+ e^{-i\underline{\kappa} \cdot \underline{x}} \tag{3.4}$$

where $\hat{e}_\lambda$ gives the polarization of the photon and for emission we consider the photon creation portion (a_κ^+) of the vector potential operator $\underline{A}$. After the interaction we have N + 1 photons of frequency ω and no free carriers. The direct recombination rate leading to photons of frequency ω due to conduction band electrons of wavevector $\underline{k}$ goes as

$$\begin{aligned} \frac{2\pi}{\hbar} & \times (\text{probability of an electron in state } \Gamma\underline{k}) \\ & \times (\text{probability of a hole in state } h \; \underline{k} - \underline{\kappa}) \\ & \times (N(\omega,t) + 1) \times |\langle v\underline{k} - \underline{\kappa} \, | H_{ep} | c\underline{k} \rangle|^2 \\ & \times \delta(E_\Gamma(\underline{k}) + E_h(\underline{k} - \underline{\kappa}) - \hbar\omega) \; . \end{aligned} \tag{3.5}$$

The matrix element is evaluated in Appendix B. We assume that the photon momentum $h\underline{\kappa}$ is small with respect to the electron momentum $h\underline{k}$ and may therefore be ignored. The total contribution to $\partial N(\omega,t)/\partial t$ is the diagrams in Fig. 22 summed over the available electron states $\underline{k}$ and the two heavy hole bands and averaged over the possible photon polarizations. Taking into account both emission and absorption, the direct recombination rate is

$$\left.\frac{\partial N(\omega,t)}{\partial t}\right|_D = \frac{2\pi}{\hbar}\sum_v\left(\frac{1}{2}\sum_\lambda\right)\sum_{\underline{k}}\left(\frac{e}{mc}\right)^2\left(\frac{2\pi c^2\hbar}{\varepsilon_\infty\omega}\right)|\hat{e}_\lambda\cdot\underline{P}_{cv}(\underline{k})|^2$$

$$\times\,\delta(E_\Gamma(\underline{k}) + E_h(\underline{k}) - \hbar\omega)$$

$$\times\left\{[N(\omega,t)+1]f_\Gamma(\underline{k})f_h(\underline{k}) - N(\omega,t)[1-f_\Gamma(\underline{k})][1-f_h(\underline{k})]\right\} \tag{3.6}$$

where the matrix element $\underline{P}_{cv}(\underline{k})$ is given in Eq. (B.4). The subscript D denotes the direct process. Averaging over the polarizations of the photon and summing over valence bands we have

$$\left.\frac{\partial N(\omega,t)}{\partial t}\right|_D = \frac{e^2}{3\pi m^2\varepsilon_\infty\omega}\int d^3k\;|P_{cv}(\underline{k})|^2\left\{N(\omega,t)[f_\Gamma(\underline{k}) + f_h(\underline{k})-1] + f_\Gamma(\underline{k})f_h(\underline{k})\right\}\delta(E_\Gamma(\underline{k}) + E_h(\underline{k}) - \hbar\omega) \tag{3.7}$$

where we have replaced the sum over $\underline{k}$ by an integral.

To justify inclusion of only recombination and absorption terms in Eq. (3.7), we consider in detail the mechanisms leading to the electron distribution just prior to recombination. The incident light pulse excites electrons across the direct gap into the conduction band. The electron distribution is at a high effective temperature as electrons can be heated by free carrier absorption and plasmon-assisted recombination.[4] The Fermi level is also raised above the conduction band edge from its equilibrium value near $E_G/2$ (see Fig. 23). These hot electrons relax within the band by interaction with the phonon distribution, achieving thermal equilibrium with the lattice within a few hundred picoseconds after the excitation is turned off.[3] The equilibrium temperature is the initial lattice temperature, as the number of electrons excited is a small fraction of the total number of electrons in the crystal. We then have an electron distribution at the lattice temperature but with a Fermi level above the conduction band edge (Fig. 24). The degree of extension of the tail of the distribution above the direct gap depends on the initial temperature. At $T \simeq 300$ K there are many electrons above E_o, with a much smaller number at lower temperatures, which shows up in the experimental results as a larger direct gap contribution to the recombination spectrum at the higher temperature. Electron-electron scatterings (rate[4] $\simeq 10^{14}$ sec^{-1}) cannot alter the overall equilibrium,so the Γ valley population is unaffected by scatterings into and out of the L valleys. We therefore ignore the effects of $\Gamma \rightarrow L$ and $L \rightarrow \Gamma$ scattering contributions to the instantaneous value of $f_\Gamma(\underline{k})$ for the moment.

The matrix element $|P_{cv}(\underline{k})|^2$ obeys the f-sum rule (see Appendix B) with

$$|P_{cv}(\underline{k})|^2 \sim \frac{3m^2}{4} [E_\Gamma(\underline{k}) + E_h(\underline{k})] \left(\frac{1}{m_o} + \frac{1}{m_h}\right) . \tag{3.8}$$

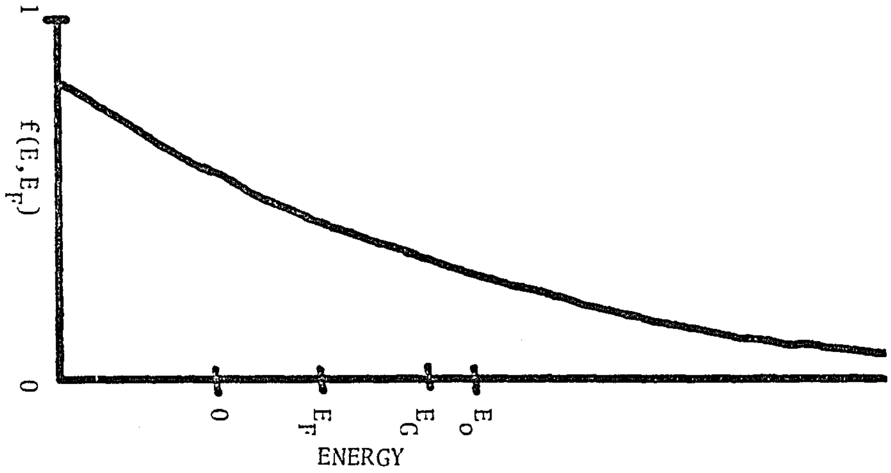

Fig. 23. Conduction Band Electron Distribution after Excitation of the Sample by a High Intensity Laser Pulse.

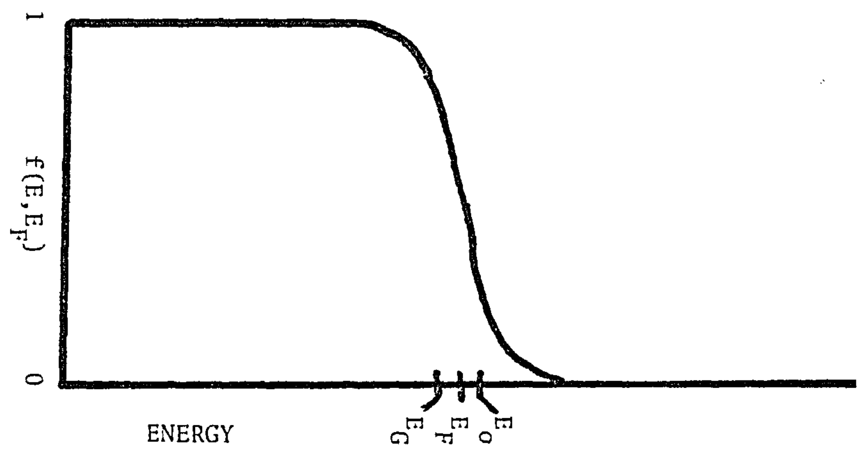

Fig. 24. Conduction Band Electron Distribution at Time $t \simeq \tau_D$ after Excitation.

Using Eq. (3.2), the argument of the δ-function in Eq. (3.7) becomes

$$\delta(E_\Gamma(\underline{k}) + E_\hbar(\underline{k}) - h\omega) = \delta(E_o + \frac{\hbar^2 k^2}{2m_o} + \frac{\hbar^2 k^2}{2m_h} - \hbar\omega) = \delta(E + E_o - \hbar\omega) \tag{3.9}$$

where we change variables from k to

$$E = \frac{\hbar^2 k^2}{2m_{BE}}$$

and define

$$m_{BE} = (\frac{1}{m_o} + \frac{1}{m_h})^{-1} .$$

In this case

$$d^3k = 4\pi k^2 dk = 2\pi(\frac{2m_{BE}}{\hbar^2})^{3/2} E^{1/2} \underline{dE}$$

and the Fermi functions are

$$f_\Gamma(\underline{k}) = f(E_o + \frac{m_{BE}}{m_o} E, E_F)$$

$$f_h(\underline{k}) = f(\frac{m_{BE}}{m_h} E, E_H)$$

where we define

$$f(X,Y) \equiv [1 + \exp \beta(X - Y)]^{-1} . \tag{3.10}$$

With these substitutions, Eq. (3.7) becomes

$$\left.\frac{\partial N(\omega,t)}{\partial t}\right|_D = \frac{e^2}{3m^2\pi\varepsilon_\infty\omega} \frac{3m^2}{4m_{BE}} 2\pi(\frac{2m_{BE}}{\hbar^2})^{3/2} \int dE(E + E_o)E^{1/2}\delta(E + E_o - \hbar\omega)$$

$$\times \Big\{N(\omega,t)[f(E_o + \frac{m_{BE}}{m_o} E, E_F) + f(\frac{m_{BE}}{m_h} E, E_H) - 1]$$

$$+ f(E_o + \frac{m_{BE}}{m_o} E, E_F) f(\frac{m_{BE}}{m_h} E, E_H)\Big\} . \tag{3.11}$$

The number of quanta per mode $N(\omega,t)$ will in general be much smaller than 1, so we drop all terms involving N. This in effect ignores all but the terms involving spontaneous emission. We take absorption into account in a phenomenological manner in a later section of this chapter. Carrying out the integral yields

$$\left.\frac{N(\omega,t)}{\partial t}\right|_D = \frac{e^2}{\hbar^2\varepsilon_\infty}\,[2m_{BE}(\hbar\omega - E_o)]^{1/2} f(E_o + \frac{m_{BE}}{m_o}(\hbar\omega - E_o), E_F)$$
$$f(\frac{m_{BE}}{m_h}(\hbar\omega - E_o),\ E_H)\ . \qquad (3.12)$$

Indirect Recombination

We now turn our attention to recombinations from the states around the L point to the valence bands. A photon of wavelength $\lambda \simeq 1.8$ μm, corresponding to the indirect band gap energy, has a wavevector $\kappa \simeq 2\pi/\lambda \simeq$ few $\times\ 10^4$ cm^{-1} while the wavevector difference k_L between the L-valley minimum and the valence band maximum is approximately $\pi/a \simeq 10^8$ cm^{-1} (a is the lattice constant). Therefore the one-photon direct process is forbidden by momentum conservation. The next higher order process involves a phonon to conserve momentum and a photon to conserve energy. The photon emission processes are shown schematically in Fig. 21 with photon absorption being the two reverse processes. The two alternatives are dependent on whether the electron-photon interaction occurs "before" or "after" the electron-phonon interaction. In the first case, the electron in state $(L,\underline{k})$ makes a virtual transition to the valence band state $(v,\underline{k})$ with emission of a photon and then scatters to valence band state $(v,\underline{k} - \underline{q})$ by either emission of a phonon of wavevector $\underline{q}$ or absorption of a phonon $-\underline{q}$. The second case corresponds to a virtual scattering of an electron from state $(L,\underline{k})$ to state $(\Gamma,\underline{k} - \underline{q})$, again with emission or absorption of a phonon, followed by a direct transition to valence band state $(v,\underline{k} - \underline{q})$ with emission of a photon. The intermediate states, being virtual, do not conserve energy, while both momentum and energy conservation hold for the initial and final electron states, the emitted photon and the phonon. Taking into account the reabsorption terms, we must consider four photon emission diagrams and four photon absorption diagrams. Representative examples are shown in Fig. 25.

The resulting expression for $\partial N(\omega,t)/\partial t$, though of the same general form as the direct recombination term, is as expected more complex. In addition to the sums over conduction band states, valence bands and polarizations, we must include sums over the four possible L valleys and, more importantly, over the possible wavevectors $\underline{q}$ of the absorbed and emitted phonons. The phonon interaction occurs through the Hamiltonian

$$H_{e\phi} = \sum_q \sum_u \left(\frac{\hbar}{2\rho\Omega_{qu}}\right)^{1/2} Q_{qu} \{a_{qu} e^{i\underline{q}\cdot\underline{x}} + a_{qu}^{\dagger} e^{-i\underline{q}\cdot\underline{x}}\} \tag{3.13}$$

where Q_{qu} is the electron-phonon coupling and $\hbar\Omega_{qu}$ is the energy of a phonon of wavevector $\underline{q}$ and type u (longitudinal or transverse optical or acoustical). We consider initially the effects due to optical phonons which are assumed to have energy $\hbar\Omega_o$ independent of q. We write the indirect recombination rate in a manner analogous to that suggested by Eq. (3.5), remembering that we must multiply our expressions involving

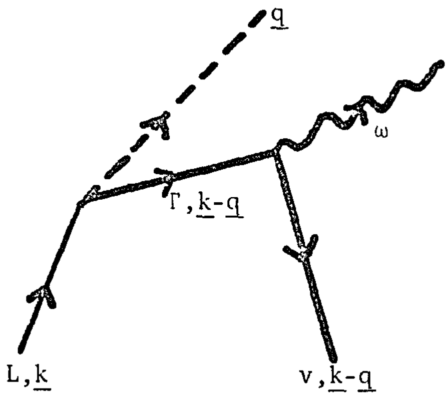

a.

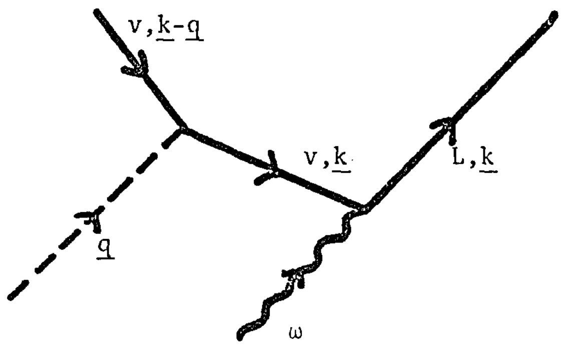

b.

Fig. 25. Typical Indirect (Phonon-Assisted) Transitions.

Emission (a) or absorption (b) of a photon.
Broken lines refer to phonons.

emission and absorption of phonons by factors involving the band edge phonon distribution function

$$\eta_q = [\exp(\beta\hbar\Omega_{qu}) - 1]^{-1} . \tag{3.14}$$

This gives

$$\left.\frac{\partial N(\omega,t)}{\partial t}\right|_I = \frac{2\pi}{\hbar}\sum_L \sum_v \sum_{\underline{k}} \sum_{\underline{q}} (\frac{1}{2} \sum_\lambda)$$

$$= \Bigg\{ \eta_o \Bigg| \frac{<v\underline{k} - \underline{q}|H_{ep}|\Gamma\underline{k} - \underline{q}><\Gamma\underline{k} - \underline{q}|H_{e\phi}|L\underline{k}>}{E_\Gamma(\underline{k} - \underline{q}) - E_L(\underline{k}) - \hbar\Omega_o}$$

$$- \frac{<v\underline{k} - \underline{q}|H_{e\phi}|v\underline{k}><v\underline{k}|H_{ep}|L\underline{k}>}{E_h(\underline{k}) + E_L(\underline{k}) - \hbar\omega}\Bigg|^2$$

$$f_L(\underline{k}) f_h(\underline{k} - \underline{q}) \delta(E_L(\underline{k}) + E_h(\underline{k} - \underline{q}) + \hbar\Omega_o - \hbar\omega)$$

$$+ (\eta_o + 1) \Bigg| \frac{<vk - \underline{q}|H_{ep}|\Gamma\underline{k} - \underline{q}><\Gamma\underline{k} - \underline{q}|H_{e\phi}|L\underline{k}>}{E_\Gamma(\underline{k} - \underline{q}) + \hbar\Omega_o - E_L(\underline{k})}$$

$$- \frac{<v\underline{k} - \underline{q}|H_{e\phi}|v\underline{k}><v\underline{k}|H_{ep}|L\underline{k}>}{E_h(k) + E_L(k) - \hbar\omega}\Bigg|^2$$

$$f_L(\underline{k}) f_h(k - q) \delta(E_L(\underline{k}) + E_h(\underline{k} - \underline{q} - \hbar\Omega_o - \hbar\omega)\Bigg\} \tag{3.15}$$

The matrix elements for the phonon interaction are discussed in Appendix B. We have again assumed that the photon momentum is negligible with respect to the electron momenta and from the beginning will also ignore $N(\omega,t)$. The sum over $\underline{k}$ is restricted to values corresponding to L point energies less than $E_o - \hbar\Omega_o$, i.e., to electron states not within a phonon energy of a Γ valley state. Any electrons that could be scattered into the central valley must be considered as part of the direct recombination process, as the electron intervalley scattering time is extremely short compared to the direct radiative lifetime. Thus, any L valley electrons of energy greater than $E_o - \hbar\Omega_o$ will be scattered with high probability into the central valley and recombine via the direct process.

The sums over L valleys and valence bands yield a factor of 8. Evaluating the matrix elements, we obtain

$$\frac{\partial N(\omega,t)}{\partial t}\bigg|_I = \frac{2\pi}{\hbar}\, 8\left(\frac{e}{mc}\right)^2 \left(\frac{2\pi c^2\hbar}{\varepsilon_\infty \omega}\right)\left(\frac{\hbar}{2\rho\Omega_o}\right) Q_o^2 \left(\frac{1}{2}\sum_\lambda\right)\sum_{\underline{k}}\sum_{\underline{q}} f_L(\underline{k}) f_h(\underline{k}-\underline{q})$$

$$\times \Bigg\{ \left| \frac{e_\lambda \cdot \underline{P}_{cv}(\underline{k}-\underline{q})}{E_\Gamma(\underline{k}-\underline{q}) + \hbar\Omega_o - E_L(\underline{k})} + \frac{e_\lambda \cdot \underline{P}_{cv}(\underline{k})}{\hbar\omega - E_h(\underline{k}) - E_L(\underline{k})} \right|^2$$

$$\times \quad \eta_o \delta(E_L(\underline{k}) + E_h(\underline{k}-\underline{q}) + \hbar\Omega_o - \hbar\omega)$$

$$+ \left| \frac{e_\lambda \cdot \underline{P}_{cv}(\underline{k}-\underline{q})}{E_\Gamma(\underline{k}-\underline{q}) + E_h(\underline{k}-\underline{q}) - \hbar\omega} + \frac{e_\lambda \cdot \underline{P}_{cv}(\underline{k})}{-E_h(\underline{k}) + \hbar\Omega_o + E_h(\underline{k}-\underline{q})} \right|^2$$

$$\times \quad (\eta_o+1)\delta(E_L(\underline{k}) + E_h(\underline{k}-\underline{q}) - \hbar\Omega_o - \hbar\omega) \Bigg\} . \tag{3.16}$$

Using the δ-functions, we find that the matrix element contributions to the two terms on the right-hand side of Eq. (3.16) are equal. Averaging over the photon polarizations and approximating the matrix elements (Appendix B), we find

$$\frac{1}{2}\sum_\lambda |M|^2 = \frac{|\underline{P}_{cv}(\underline{k}-\underline{q})|^2}{3[E_\Gamma(\underline{k}-\underline{q}) + E_h(\underline{k}-\underline{q}) - \hbar\omega]^2} \quad . \tag{3.17}$$

Rewriting the Fermi functions in the notation of Eq. (3.10) we have

$$\left.\frac{\partial N(\omega,t)}{\partial t}\right|_{I} = \frac{16\pi^2}{3}\frac{c^2}{m^2}\frac{\hbar Q_o^2}{\varepsilon_\infty \rho \Omega_o \omega}\sum_{\underline{k}}\sum_{\underline{q}}\frac{|P_{cv}(\underline{k}-\underline{q})|^2}{[E_\Gamma(\underline{k}-\underline{q}) + E_h(\underline{k}-\underline{q}) - \hbar\omega]^2}$$

$$\times \Big\{\delta(E_L(\underline{k}) + E_h(\underline{k}-\underline{q}) + \hbar\Omega_o - \hbar\omega) n_o f(E_L(\underline{k}),E_F) \; f(\hbar\omega-\hbar\Omega_o - E_L(\underline{k}),E_H)$$

$$+ \delta(E_L(\underline{k}) + E_h(\underline{k}-\underline{q}) + \hbar\Omega_o - \hbar\omega)(n_o+1) f(E_L(\underline{k}),E_F) \; f(\hbar\omega+\hbar\Omega_o - E_L(\underline{k}),E_H)\Big\} . \tag{3.18}$$

The only q-dependences are thus in the energy denominator, the matrix elements, and the δ-functions.

The summation over $\underline{q}$ can be converted to an integral over $\underline{s} = \underline{k} - \underline{q}$, yielding

$$S = \left[\frac{m_h}{m_{BE}}(\hbar\omega\pm\hbar\Omega_o - E_L(\underline{k})) + E_o - \hbar\omega\right]^{-2}\left(\frac{2m_h}{\hbar^2}\right)^{3/2} \frac{\hbar\omega\pm\hbar\Omega_o - E_L(\underline{k})}{(2\pi)^2}\left[E_o + \frac{m_h}{m_{BE}}[\hbar\omega \pm \hbar\Omega_o - E_L(\underline{k})]\right] \tag{3.19}$$

where the upper (lower) sign applies to phonon absorption (emission) in Eq. (3.18). Substituting from Eq. (3.19) into Eq. (3.18), converting to an integration and changing variables from $\underline{k}$ to $E = E_L(\underline{k}) = E_G + \frac{\hbar^2}{2m_c}k^2$, the integrand becomes

$$F(E_L(\underline{k}))k^2dk \to \frac{1}{2}\left(\frac{2m_c}{\hbar^2}\right)^{3/2} F(E)(E - E_G)^{1/2}dE$$

and we have

$$\left.\frac{\partial N(\omega,t)}{\partial t}\right|_{I} = \frac{2}{\pi^2}\frac{e^2}{\hbar^5}(m_c m_h)^{3/2}\frac{Q_o^2}{\varepsilon_\infty \rho m_{BE}\Omega_o \omega}$$

$$\times \quad \{n_o I(\omega,-\Omega_o) + (n_o + 1) I(\omega,+\Omega_o)\} \tag{3.20}$$

where

$$I(\omega,\pm\Omega_o) = \int dE\ f(E,E_F) f(\hbar\omega \pm \hbar\Omega_o - E, E_H)(E - E_G)^{1/2}$$
$$\times \frac{(\hbar\omega \pm \hbar\Omega_o - E)^{1/2}[E_o + \frac{m_h}{m_{BE}}(\hbar\omega \pm \hbar\Omega_o - E)]}{[\frac{m_h}{m_{BE}}(\hbar\omega \pm \hbar\Omega_o - E) + E_o - \hbar\omega]^2} . \tag{3.21}$$

The lower limit to the integration is $E_L(\underline{k} = \underline{k}_L) = E_G$, and the upper limit is set by $E_L(\underline{k}) < \hbar\omega \pm \hbar\Omega_o$ or $E_L(\underline{k}) < E_o - \hbar\Omega_o$, whichever is smaller.

In this calculation we considered only the contribution due to optical phonons. To account for acoustical phonons we must include the q dependence of Q_{qu} and $h\Omega_{qu}$. The phonon wavevectors of interest are $\underline{q} \sim \underline{k}_L$, so we take advantage of the approximations for acoustical phonons

$$Q_{\underline{k}_L} \sim Q_o$$

$$\hbar\Omega_{\underline{k}_L} \sim \hbar\Omega_o \tag{3.22}$$

and represent the acoustical-phonon-assisted indirect recombination by the same expression obtained for optical phonons.

Combined Photoluminescence

The number of photons emitted per unit frequency goes as

$$S(h\omega)d\omega = g(\omega)N(\omega)d\omega \tag{3.23}$$

where $g(\omega)$ is the photon density per unit frequency

$$g(\omega) = \frac{n^3\omega^3}{2\pi^2c^3} \tag{3.24}$$

and

$$N(\omega) = \int_0^\infty dt\, \frac{\partial N(\omega,t)}{\partial t} \quad . \tag{3.25}$$

The excitation for the three lower intensities used in our experiments[20] was produced by a pulse from a free-running Nd:glass laser with pulse-width $\hat{t} \simeq 200$ μsec. This is longer than the longest lifetime of importance, so a steady-state carrier density situation is reached during most of the period that the excitation pulse is on. We therefore ignore effects concerning the front and back edges of the pulse as having negligible contribution to the observed luminescence and assume that we may take $\partial N(\omega,t)/\partial t$ as constant over the time period of interest. The time integration is then trivial, resulting in

$$S(\hbar\omega) \sim g(\omega)\frac{\partial N(\omega,t)}{\partial t} \tag{3.26}$$

where we assume one average Fermi level throughout the sample for all times.

For the highest intensity, produced with an excitation pulse of width $\hat{t} \simeq 10^{-11}$ sec, much shorter than times of interest, we assume the carriers are excited at $t = 0$ and diffuse into the sample until recombining, with the effective Fermi level for the direct (indirect) process chosen by the approximate densities that would exist after the direct (indirect) lifetime over the portion of the sample within one direct (indirect) diffusion length of the front surface. This process is considered among the diffusion effects accounted for in the next section.

Thus, for both cases, the flux produced at the position of carrier recombination has contributions from both the direct and indirect processes

$$S(h\omega) \sim g(\omega) \left[\left.\frac{\partial N(\omega)}{\partial t}\right|_D + 2 \cdot \left.\frac{\partial N(\omega)}{\partial t}\right|_I \right] \tag{3.27}$$

given by Eqs. (3.12) and (3.20) respectively. The factor of 2 accounts for optical and acoustical phonon contributions to the indirect luminescence.

<u>Radiative Recombination: Diffusion Effects</u>

The initial excitation of the sample by the incident laser pulse occurs within the first few micrometers of the front surface, yielding the density as a function of distance into the sample

$$n(z,t=0) = N_o \exp(-\alpha_o z) \tag{3.28}$$

where α_o is the absorption coefficient of the incident light ($\alpha_o \simeq 10^4$ cm^{-1} for $\lambda \simeq 1.06$ μm). This is an extremely inhomogeneous distribution that immediately begins to diffuse into the sample in an attempt to create a uniform density throughout the sample. The diffusion constant at T = 300 K is 60 cm^2 sec^{-1}, so, for times on the order of the direct radiative lifetime $T_D \simeq$ few × 10^{-8} sec, the carriers have diffused well into the sample. At the position of carrier recombination, the photon flux is given by Eq. (3.27). However, the absorption coefficient for the direct photoluminescence is $\alpha_o \simeq 10^3$ cm^{-1}, so the reabsorption of the emitted radiation is significant. Thus, before final results are taken from Eq. (3.27), it is necessary to account for diffusion and reabsorption processes.

For the carriers involved in indirect recombination this is a relatively easy matter to resolve. The indirect lifetimes can be calculated following the approaches of van Roosbroeck and Shockley[23] and of Ryvken.[24] The carrier radiative lifetime for high excitation levels (carrier density $n \gg n_e$, the intrinsic carrier density) is given by

$$\tau = \frac{n_e^2}{Rn} \tag{3.29}$$

where R is the recombination rate per unit volume

$$R = \int P(\omega)\rho(\omega)d\omega \ . \tag{3.30}$$

$P(\omega)$ is the probability of absorption of a photon of frequency ω per unit time and $\rho(\omega)d\omega$ is the photon density over the frequency range $d\omega$. This was shown by van Roosbroeck and Shockley to be

$$R = 1.57 \times 10^{13} \left(\frac{T}{300}\right)^4 \text{ sec}^{-1} \text{ cm}^{-3} \ . \tag{3.31}$$

The intrinsic carrier density is given by the extent of the tail of the unexcited Fermi distribution. The Fermi level for the unexcited distribution is near the middle of the band gap, so the carrier density is given by[25]

$$n_e = 4 \left(\frac{k_B T}{2\pi h}\right)^{3/2} (m_c m_h)^{3/4} \exp(-E_G/2k_B T)$$

$$= 1.45 \times 10^{15}\ T^{3/2} \exp(-3850/T)\ \text{cm}^{-3}\ . \tag{3.32}$$

Here we have ignored the insignificant contribution from the Γ valley.

The excited carrier density can be determined from the Fermi level by

$$n = 4 \cdot \frac{1}{(2\pi)^3} \int_{E_L > E_G} d^3k [1 + \exp(\beta(E_L(\underline{k}) - E_F))]^{-1} \tag{3.33}$$

$$= 1.13 \times 10^{15}\ T^{3/2} F_{1/2}\ (\beta(E_F - E_G))$$

where the integral is over the available states in one of the L valleys and $F_k(\eta)$ is the Fermi-Dirac function[26] of order k

$$F_k(\eta) = \int_0^\infty dx\ x^k [1 + \exp(x - \eta)]^{-1}\ . \tag{3.34}$$

The Γ valley contribution to n is down by three orders of magnitude from Eq. (3.33).

Substituting Eqs. (3.31)(3.32)(3.33) into Eq. (3.29), we find that the indirect recombination lifetime is

$$\tau_I = 4.80 \times 10^5 \left(\frac{300}{T}\right)^{5/2} \exp(-7700/T) [F_{\frac{1}{2}}(\beta(E_F - E_G))]^{-1}\ \text{sec.} \tag{3.35}$$

We consider the action of the diffusion as if it were due to the motion of one type of carrier, despite the existence of two carrier types with different diffusion constants. As we have nearly equal densities of electrons and holes, any tendency for the two carrier distributions to separate will be counteracted by their Coulomb attraction. Thus, the electron and hole densities are related by

$$n_e(z,t) = n_h(z,t)$$

for all times over the entire sample. This process is known as ambipolar diffusion and occurs with an effective diffusion constant [27]

$$D = \frac{u_e D_h + u_h D_e}{\mu_e + \mu_h} = \frac{2D_e D_h}{D_e + D_h} \tag{3.36}$$

where D_e and D_h are the electron and hole diffusion constants and[22,27]

$$\mu_e = 3800 \left(\frac{300}{T}\right)^{5/3} \quad \text{cm V}^{-1}\text{ sec}^{-1}$$

$$\mu_h = 1820 \left(\frac{300}{T}\right)^{7/3} \quad \text{cm V}^{-1}\text{ sec}^{-1}$$

$$D_{e,h} = \frac{k_B T}{e} \mu_{e,h}$$

$$D = \frac{2k_B T}{e}\left(\frac{e\ h}{\mu_e + \mu_h}\right)$$

$$= 358 \left(\frac{300}{T}\right)^{4/3} \left[3.8 + 1.82 \left(\frac{300}{T}\right)^{2/3}\right]^{-1} \quad \text{cm}^2\text{ sec}^{-1}. \tag{3.37}$$

The diffusion length of the carriers is given by

$$l_l = (D\tau_l)^{1/2} . \tag{3.38}$$

Values of the indirect lifetimes and diffusion constants are given in Table III for an excitation leading to a density of $n \simeq 5 \times 10^{18}$ cm^{-3} over the entire sample. The diffusion lengths are longer than the sample thickness, so the carrier distribution will be essentially uniform over the sample

$$n(z) = n_I = \text{constant.} \tag{3.39}$$

The photon flux emitted from the sample will then go as

$$F(\hbar\omega, z < 0) = \frac{1}{L}\int_0^L dz\; S(\hbar\omega) n_I \exp(-\alpha(\omega)z)$$

$$= n_I S(\hbar\omega) \frac{1 - \exp(-\alpha(\omega)L)}{\alpha(\omega)L} \tag{3.40}$$

where $\alpha(\omega)$ is the absorption coefficient for light of frequency ω,[28] and by implication we consider only the contribution to $S(\hbar\omega)$ resulting from the indirect recombinations.

The case of the direct recombination terms is again more complicated. The diffusion lengths corresponding to direct lifetimes ($\tau_D \simeq 40$ nsec) are on the order of 20 μm. Thus, the distribution when direct processes are important will be far from uniform. For example, if $l_D = 20$ μm, the theory that we develop here predicts the carrier distribution shown in Fig. 26. This must be numerically integrated over the sample thickness to find the effect of the reabsorption.

The evolution of the carrier density is described by the continuity equation

$$\frac{\partial n}{\partial t} + \frac{1}{e}\nabla \cdot \underline{J} = 0 \tag{3.41}$$

Table III. Diffusion Lengths and Lifetimes.

T (K)	D (cm^2/s)	τ_I (μs)	τ_D (ns)	ℓ_D (μm)
300	64	2.7	37	15.3
231	85	0.6	46	19.7
174	115	5.3	37	20.5

T = temperature; D = diffusion constant; τ_I = indirect recombination lifetime; τ_D = direct recombination lifetime; ℓ_D = direct diffusion length = $(D\tau_D)^{\frac{1}{2}}$.

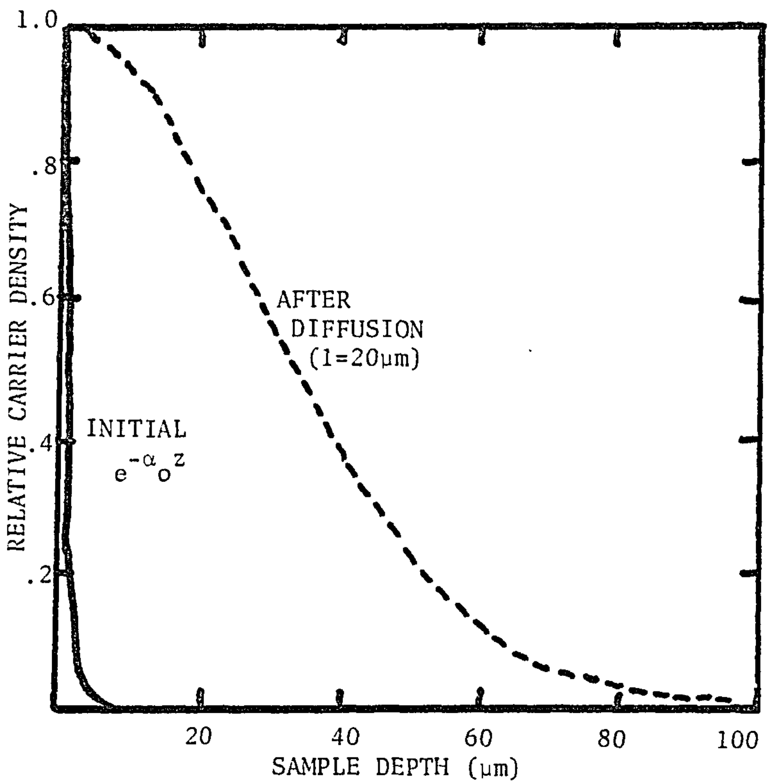

Fig. 26. Relative Electron Densities as a Function of Distance from the Front Surface of the Sample.

Solid line represents time t = 0; broken line represents time t ≈ τ_D (after diffusion into the sample).

where the current density contains a diffusion term

$$\underline{J} = -eD\nabla n \tag{3.42}$$

proportional to the carrier density gradient. By phenomenologically including a term describing recombination, we arrive at the diffusion equation

$$\frac{\partial n}{\partial t} = -\frac{n - n_e}{\tau} + D\nabla^2 n \tag{3.43}$$

where n_e is the equilibrium carrier density, τ the recombination lifetime, and D the ambipolar diffusion constant. The primary process affecting the overall carrier density for the time scales we are interested in is indirect recombination. For purposes of diffusion calculations for the direct recombination, we need not consider the recombination term in Eq. (3.43), which results only in an overall factor $\exp(-t/\tau_I)$ multiplying the final result. For $t \approx \tau_D$, the correction may be ignored.

Solution of Eq. (3.43) for an infinite one-dimensional medium with the initial condition that the density at t = 0 is given by $n(\xi,0)$ yields

$$n(z,t) = \frac{1}{2\sqrt{\pi Dt}} \int_{-\infty}^{\infty} d\xi \; n(\xi,0) \; \exp[-(\xi - z)^2/4Dt]. \tag{3.44}$$

We need consider only a one-dimensional model, as diffusion parallel to the surface will not significantly affect the density for times of interest, as the incident beam diameter is much greater than the diffusion length.

For a semi-infinite medium ($0 < z < \infty$) such as a thick sample ($L \gg \sqrt{D\tau}$) we assume that carriers that diffuse toward the front surface ($z = 0$) reflect back into the sample. This will occur for high-quality sample surfaces for which surface recombination can be ignored. In this case we have

$$n(z,t) = \frac{1}{2\sqrt{\pi D t}} \int_0^{\infty} d\xi \; n(\xi,0) \left[\exp\left(\frac{-(\xi-z)^2}{4Dt}\right) + \exp\left(\frac{-(\xi+z)^2}{4Dt}\right)\right]. \tag{3.45}$$

The flux emitted from the sample is then proportional to the integral over the sample of the carrier density $n(z,t)$ and the flux emitted at the position of recombination $S(\hbar\omega)$ with the reabsorption taken into account

$$F(\hbar\omega) = \int_0^{L} dz \; n(z,t) \; S(\hbar\omega) \; \exp[-\alpha(\omega) z]. \tag{3.46}$$

Experimental Fit

A schematic diagram of the experimental apparatus is shown in Fig. 27. The laser operates in either a free-running (pulsewidth $\hat{t} \approx$ 200 μsec) or mode-locked ($\hat{t} \approx 10$ psec) configuration; by focusing and filtering the beam, incident intensities to over 10^9 W/cm^2 can be achieved. The focused beam is passed through a hole in an aluminum coated spherical mirror mounted in a small dewar and impinges on the sample, which is cooled by connection to the dewar cold finger. The various temperatures were obtained by room temperature (295 K), liquid

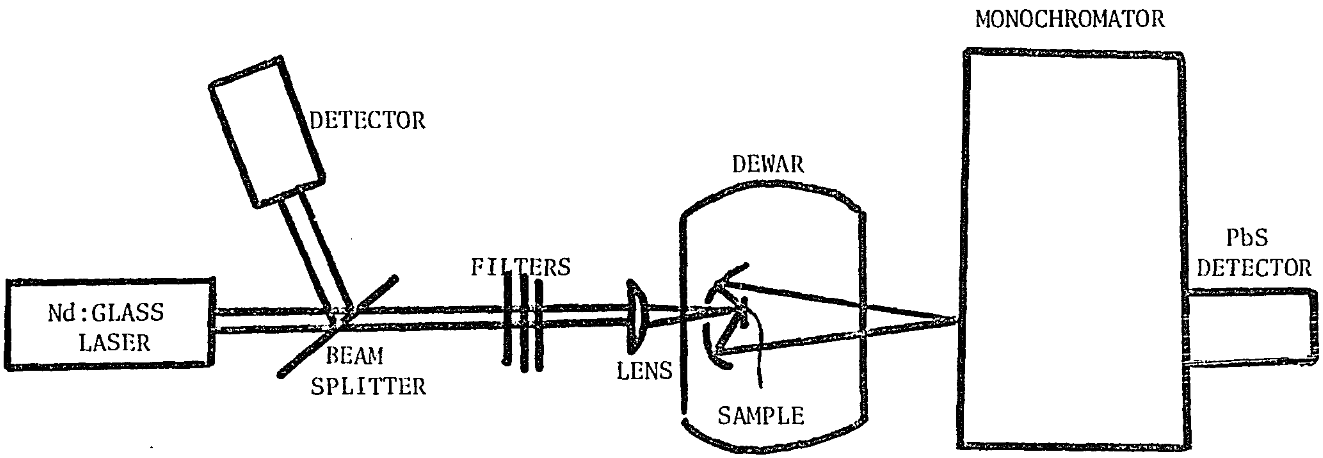

Fig. 27. Diagram of the Experimental Apparatus for Observation of Photoluminescence.

nitrogen (174 K), and a mixture of dry ice and acetone (231 K). The temperatures were measured with a copper-constantan thermocouple placed at the sample site and, in the cases of the two lower temperatures, are higher than the coolant equilibrium temperature owing to inefficiencies inherent in the coupling of the sample to the cold finger. The luminescence emitted by the sample is collected by the mirror and focused onto a 100-μm entrance slit of a 0.25-m Jarrell-Ash monochromator. The output of the monochromator is monitored by a PbS detector biased at 300 V. The bias voltage sweeps carriers created by the incident recombination radiation onto a storage capacitor, which is read by a peak detector circuit. The incident intensity is proportional to the output voltage from the detector circuit. To reduce the noise component introduced by the intense Nd:glass beam, a special set of blocking filters with 0.1% transmission at 1.06 μm was placed between the sample and the monochromator. The incident pulse energy is monitored by a p-i-n Si photodiode. Absolute calibration of the photodiode is accomplished with a Hadron thermopile and energy meter. Figure 28 shows the experimental points obtained, corrected for the response of the monochromator detector system.

We have determined the direct lifetimes by considering the high intensity experimental results, obtained using mode-locked pulses of pulsewidth $\hat{t} \simeq 10^{-11}$ sec. The initial carrier distribution given by Eq. (3.28) diffuses into the sample with an effective diffusion length

$$\ell(t) = (Dt)^{\frac{1}{2}}. \tag{3.47}$$

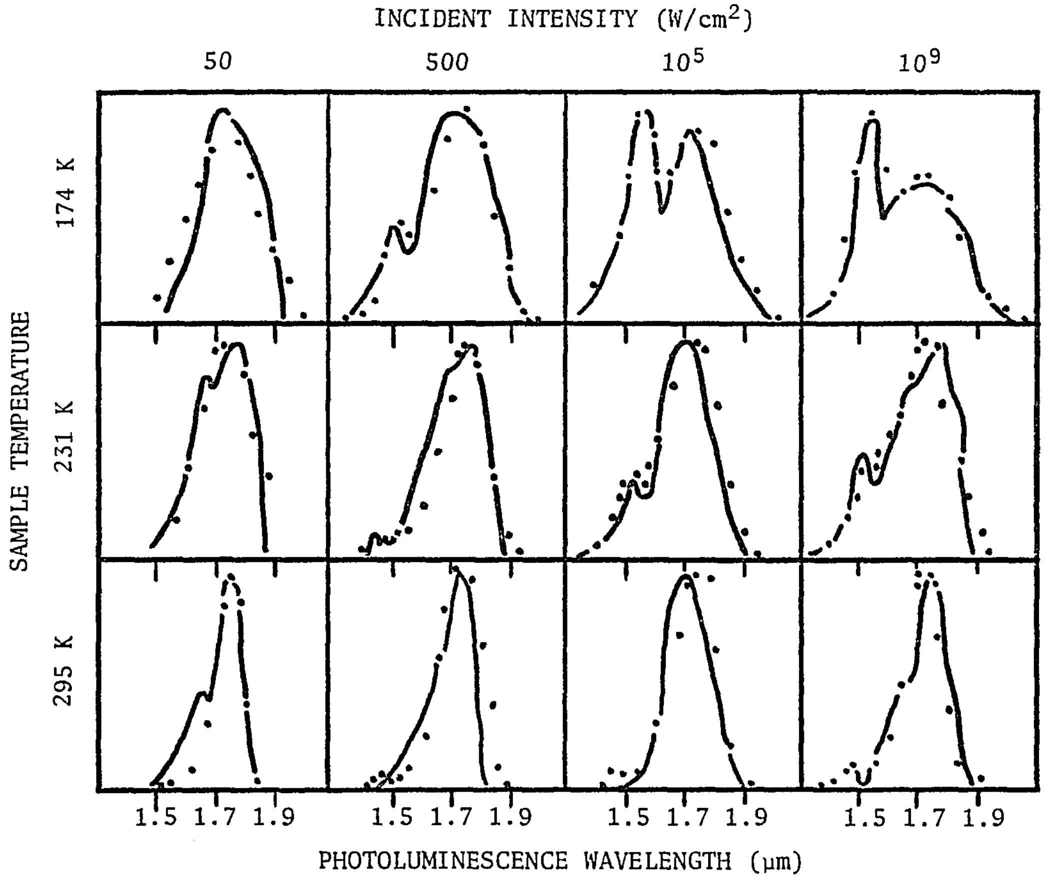

Fig. 28. Photoluminescence Intensity (Arbitrary Units) vs. Recombination Wavelength (μm).

Experimental points (•) and theoretical fit (solid lines) at temperatures 174 K, 231 K, and 295 K for incident intensities 50, 500, 10^5, and 10^9 W/cm^2.

The electron distribution at any given time can be represented by an average Fermi level $E_F(t)$, which is calculated by approximating the total number of carriers produced by the incident pulse per unit area. Dividing this by $\ell(t)$ gives the average density over the diffusion length as a function of time. By inverting Eq. (3.33), we find $E_F(t)$. For an incident intensity of 10^9 W/cm^2, approximately $N_L = 5.3 \times 10^{16}$ carriers/cm^2 are excited and diffuse throughout the sample within a time τ_I. The sample thickness is 100 μm, so the density is about 5.3×10^{18} cm^{-3} by the time indirect recombination becomes important. At T = 295 K this corresponds to a Fermi level $E_F^I = 0.68$ eV for the indirect process. From calculations of $F(\hbar\omega)$ including diffusion we obtain a value P_I for the flux at the peak of the indirect distribution. By considering various possible Fermi levels E_F^D, we calculate the ratio R of the number of electrons that can recombine via the direct process $(E > E_O - \hbar\Omega_O)$ to the number that recombine via the indirect process $(E < E_O - \hbar\Omega_O)$ and the flux P_D at the peak of the direct distribution. Then we require that $R \cdot P_D/P_I$ equal the ratio of the heights of the direct and indirect components of the experimentally observed spectra. This determines the average Fermi level for the direct recombination. For T = 295 K, this yields $E_F^D = 0.77$ eV, which corresponds to a density $n = 3.5 \times 10^{19}$ cm^{-3}. Dividing n into N_L gives the direct diffusion length and thus the direct lifetime. These values are included in Table III. The lifetime calculated here for 295 K is most likely reasonable. However, for the other two temperatures the peaks of the direct contributions are nearly lost in the short-wavelength tail of the indirect spectra, and the Fermi levels are probably not as high as calculated by this model.

The equations were integrated numerically to yield the curves of Fig. 28. The lifetimes and diffusion lengths for the different temperatures were given in Table III; Table IV indicates the Fermi levels used in the calculations. As can be seen in Fig. 28, the fit is quite good. The two-humped shape of the indirect spectra reflects the onset of phonon emission and absorption terms at $\hbar\omega = E_G - \hbar\Omega_O$ and $\hbar\omega = E_G + \hbar\Omega_O$, respectively. These are washed out in the observed spectra owing to the limits of validity of the assumptions of definite energies for the electrons and monoenergetic phonons and the resolution of the experimental observations.

Table IV. Fermi Levels in eV for the Direct Photoluminescence for Different Temperatures and Incident Intensities.

T (K)	I_O (W/cm^2) 50	500	10^5	10^9
300	0.66	0.69	0.76	0.77
231	0.66	0.69	0.77	0.78
174	0.66	0.72	0.79	0.80

A Germanium Laser?

The applicability of the preceding sections to inducing a laser transition across the direct gap in germanium comes down in the end to a rather simple question: Can we produce a high enough excitation level to create the population inversion necessary to achieve lasing? To guarantee that the required population inversion exists, we must ensure that the electron and hole Fermi levels extend into the direct conduction valley and valance band, respectively (Fig. 29). This creates degenerate electron and hole distributions at the appropriate optically coupled "laser" states. This criterion has not been satisfied for the electron Fermi level in our experiments, as the highest Fermi level achieved falls a few meV short. However, some encouragement comes from the realization that our sample is thick ($\sim$100 μm). Working with thinner samples will allow us to push the Fermi level up to the required position in the conduction band.

In addition to the Fermi level, we must consider such factors as the oscillator strength and the radiative quantum efficiency of the transition. These will in the final analysis determine whether the germanium laser is possible. Current indications are that this venture will be unsuccessful. However, the number of different semiconductors that have been made to lase under a wide variety of conditions provides encouragement. Several experiments are now being started by van Driel[29] at the University of Toronto to consider such important questions as the ratio of radiative to nonradiative recombination. A definitive statement on the feasibility of the Ge laser awaits the results of these experiments.

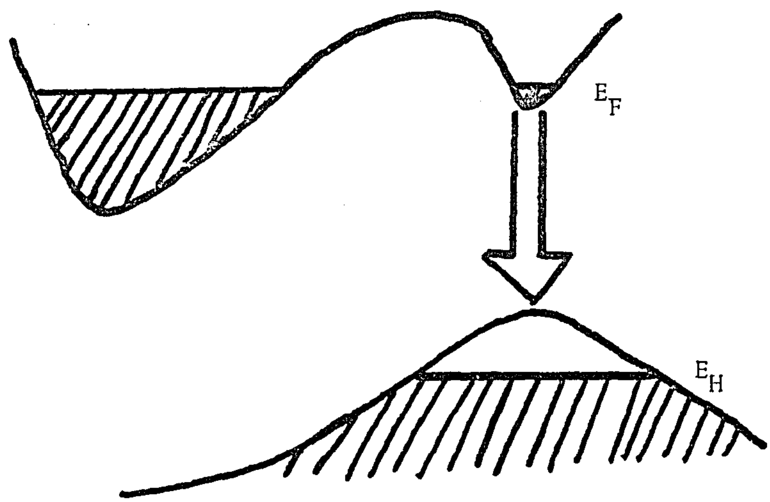

Fig. 29. Representation of the Carrier Degeneracies for E_H in the Valence Band and E_F in the Central Conduction Valley.

The coupled laser states are now completely filled with electrons (cross-hatched regions) in the conduction band and holes (blank regions) in the valence band.

CHAPTER 4

CONCLUSIONS

So what have we been able to learn that justifies the time and effort expended on this series of forays into the far reaches of high intensity infrared semiconductor physics? The radiative recombination exercise is, in the short run, academic, attempting to produce a laser in a material that to date has not worked out as an active medium. The transmission experiments are merely a compendium of information on what happens to a given pulse under given conditions in a given sample. But in the long run these experiments are much more than a way to tie up money, equipment, and manpower. The present is closely tied to semiconductors, and the future will be even more so, as semiconductor technology becomes ever more important to the increasingly fast-paced way of life we follow. Considering the place of semiconductors in what will soon be the essence of our everyday existence, we have the need to provide a sound theoretical understanding of basic processes in semiconductors on a general level. This understanding will be provided only in small steps, slowly expanding until someday everything will be tied together into a basic explanation of the microscopic and macroscopic processes that occur. Until then, the efforts will be in narrowly delimited ranges, with attempts to produce theoretical approaches explaining the particular branch of semiconductor physics in which the researcher finds himself involved. The experiments and theory described in the previous chapters are an attempt within such a narrow range.

Before ESSM, there were no comprehensive "first-principles" theoretical studies of the ultrafast electron plasma response of the elemental group IV semiconductors, which are among the most important to modern technology. ESSM abounds in approximations in its description of band structure, band shape, and all of the little details that enter into its calculations. That its results match the work of Smirl and coworkers is in part due to the interplay between experiment and theory that went into the model proposed. The quality of the theoretical fit to the pressure data presented here must be a source of pride to the proponents of ESSM in that a model based on band gap temperature effects fits well to an equivalent "semiconductor" produced by hydrostatic pressure. The failure of the prediction of the pulsewidth dependences, in the face of the extreme sensitivity of the theoretical result to the various coupling constants, cannot really be seen as a failure of any great magnitude. The coupling constants are not known to an accuracy that definitely rules out any particular choice of theoretical pulsewidth dependence. However, a definitive pulsewidth experiment, for which we have provided the groundwork, coupled with a slightly better, i.e., less approximated, theory, the work on which we have justified here, could lead to another method of determining the coupling constants by doing just what has been done here, adjusting the coupling constants in the theory until the theoretical curves match the experimental results.

The primary requirement from the experimental perspective is to provide a better control of the laser pulses. This may be beyond the capability of most glass laser systems. Perhaps working with a mode locked Nd:YAG laser, sacrificing pulse shortness (25 psec compared to 5-10 psec) for better statistics (30 pulses per minute with a box-car integrator) would provide the second pulsewidth necessary for the experiment. It is interesting that little work in transient semiconductor plasma response has been carried out with a YAG laser. An effort of this type would pay dividends in statistics, reproducibility, and energy over Nd:glass. The new generation of mode-locked YAG lasers now appearing on the market may provide the impetus for such an effort.

The thin film characteristic study of Chapter 2 and the photoluminescence work of Chapter 3 provide information in another, perhaps more important, area. Combining the results here with work on other semiconductors and with the theory of ESSM would advance the knowledge regarding lifetimes and diffusion of excited carriers. Additional information would have to be supplied in treatments of doped semiconductors, surface effects,and the effects of semiconductor heterojunctions. An example of the possible applications is in the field of heterojunction physics. Semiconductor heterojunctions are currently being intensively studied for applications in solar energy conversion, light emitting diodes, and many other high technology devices. A great deal of effort is being expended in trying to understand electron transport properties in the vicinity of the heterojunction. These properties are significantly affected by lifetimes and diffusion effects.

The previous three-plus chapters have dabbled at the frontiers of semiconductor physics, providing a small and specialized glimpse into the workings of nature. What was learned will be revised many times before a general understanding of ultrafast processes is reached. In the long run this may even appear to be but a short trip down a dead end road. That it is a contribution to further progress toward the end of the road it follows justifies the time involved.

APPENDIX A

VAPOR PHASE EPITAXY

The technique of vapor phase epitaxial deposition provides a method of producing inexpensive and ultrathin (∿ a few μm) germanium samples. The technique involves a disproportionate reaction with GeI_2. The chemical reactions and the temperatures at which they take place are:

$$Ge + I_2 \rightleftarrows GeI_2 \qquad 650\ C$$

$$2GeI_2 \rightleftarrows Ge + GeI_4 \qquad 325\ C$$

Additional GeI_2 appears if hydrogen is used as the carrier gas:

$$H_2 + I_2 \longrightarrow 2HI$$

$$2HI + Ge \longrightarrow H_2 + GeI_2$$

The reactions occur in a furnace-vessel shown in Fig. 30. The carrier gas, either H_2 or He or a mixture of the two, picks up I_2 vapor and carries it into the germanium. The reaction forms GeI_2 with very high efficiency, which is then carried into the section containing the GaAs substrate. The disproportionate reaction occurs due to the temperature gradient. The GeI_4 is removed by the carrier gas while the Ge deposits on the GaAs substrate. The growth rate of the Ge can be varied from about .5 to greater than 5 μm per hour by varying the assorted

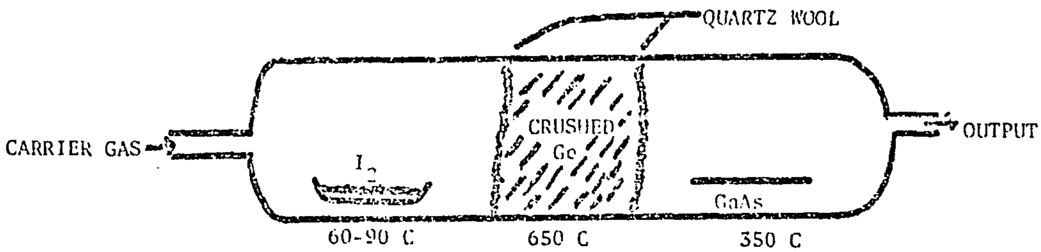

Fig. 30. Schematic of Apparatus for Producing Vapor Phase Epitaxially Grown Germanium Films on Gallium Arsenide Substrates.

parameters. The rate is relatively well reproducible using the same input parameters from one run to the next.

I wish to include here a special thank you to Dr. F. C. Jain of the Electrical Engineering Department of the University of Connecticut for his collaboration on the thin Ge film project.

APPENDIX B

MATRIX ELEMENTS

As a representative example of the matrix elements we must take into account in calculating the recombination rates, we consider the element for the emission diagram in Fig. 25. This includes contributions from both phonon and photon interactions with the electron and hole. The interaction is second order, beginning with a system containing one electron in state $(L,\underline{k})$, one hole in $(v, \underline{k} - \underline{q})$, and no phonons or photons. The electron makes a virtual transition to the state $(\Gamma,\underline{k} - \underline{q})$ by emission of a phonon of wavevector $\underline{q}$ and then recombines with the hole, emitting a photon of frequency ω, resulting in a final system with one phonon, one photon, and no free carriers. The matrix element for this process is

$$M = \frac{\langle v,\underline{k} - \underline{q}|Hep|\Gamma\underline{k} - \underline{q}\rangle\langle\Gamma\underline{k} - \underline{q}|He\phi|L,\underline{k}\rangle}{E_\Gamma(\underline{k} - \underline{q}) + \hbar\Omega_o - E_L(\underline{k})} \qquad (B.1)$$

where Hep and Heϕ are the Hamiltonians for the electron-photon and electron-phonon interactions, given by Eqs. (3.4) and (3.13) respectively. In writing the intermediate state energy denominator we assume an optical phonon with $\underline{q} \sim \underline{k}_L$ and energy $\hbar\Omega_o$.

For the electron-phonon interaction we have (longitudinal optical phonon emission)[21]

$$\begin{aligned} Me\phi &= \langle \Gamma \underline{k} - \underline{q} | He\phi | L\underline{k} \rangle \\ &= \langle \Gamma \underline{k} - \underline{q} | \sum_{q'} \left(\frac{\hbar}{2\rho\Omega_o}\right)^{1/2} Q_o a^{\dagger}_{q'o} e^{-i\underline{q}'\cdot\underline{x}} | L\underline{k} \rangle \\ &= \left(\frac{\hbar}{2\rho\Omega_o}\right)^{1/2} Q_o (n_o + 1)^{1/2} \end{aligned} \tag{B.2}$$

while for the electron-photon interaction (photon emission)

$$\begin{aligned} Mep &= \langle v\underline{k} - \underline{q} | Hep | \Gamma \underline{k} - \underline{q} \rangle \\ &= \langle v\underline{k} - \underline{q} | \left(\frac{e}{mc}\right) \left(\frac{2\rho c^2 \hbar}{\varepsilon_\infty \omega}\right)^{1/2} (\hat{e}_\lambda \cdot \underline{p})\ a^{\dagger}_{\kappa} e^{-i\underline{k}\ \underline{x}} | \Gamma \underline{k} - \underline{q} \rangle \\ &= \left(\frac{e}{mc}\right) \left(\frac{2\pi c^2 \hbar}{\varepsilon_\infty \omega}\right)^{1/2} (N(\omega) + 1)^{1/2}\ \hat{e}_\lambda \cdot \underline{P}_{cv}(\underline{k} - \underline{q}) \end{aligned} \tag{B.3}$$

where we ignore the photon momentum $\underline{\kappa}$ with respect to electron momenta and define

$$\underline{P}_{cv}(\underline{k}) = \langle v\underline{k} | \underline{p} e^{-i\underline{\kappa}\cdot\underline{x}} | \Gamma \underline{k} \rangle = \underline{P}^{*}_{cv}(\underline{k}) \ . \tag{B.4}$$

The average over photon polarizations $\frac{1}{2} \sum_{\lambda} \hat{e}_\lambda \cdot \underline{P}_{cv}(\underline{k})$ leaves $|P_{cv}(\underline{k})|$. The $\underline{P}_{cv}$ obey an f-sum rule

$$\frac{2}{m} \sum_{v} \frac{P^{\alpha}_{cv}(\underline{k})\ P^{\beta}_{cv}(\underline{k})}{-E_v - E_c} = \delta_{\alpha\beta} - \frac{2m}{\hbar^2} \frac{\partial^2 (Ec+Ev)}{\partial k_\alpha \partial k_\beta} \ . \tag{B.5}$$

Summing over the valence bands and the components α of $\underline{P}_{cv}$ we obtain for $\Gamma \to v$ transitions

$$|P_{cv}(\underline{k})|^2 \sim \frac{3}{4} \frac{m^2}{m_{BE}} [E_\Gamma(\underline{k}) + E_h(\underline{k})] \tag{B.6}$$

and for $L \rightarrow v$ transitions

$$|P_{cv}(\underline{k})|^2 \sim \frac{3m^2}{4}\,[E_L(\underline{k}) + E_h(\underline{k})]\left(\frac{1}{m_c} + \frac{1}{m_h}\right) \quad . \tag{B.7}$$

As the matrix element for the process we consider in Eq. (B.1) (Fig. 21b) is much larger than for the process in which the virtual phonon emission occurs first (Fig. 21a) while the energy denominator is smaller, the dominant terms in Eq. (3.16) are those involving $\underline{P}_{cv}(\underline{k}-\underline{q})$ and we ignore the terms involving $\underline{P}_{cv}(\underline{k})$.

The δ-function governing photon and phonon emission is $\delta(E_L(\underline{k}) + E_H(\underline{k}-\underline{q}) - \hbar\Omega_o - \hbar\omega)$. Using this in Eq. (A.1) we see the energy denominator is

$$E_\Gamma(\underline{k}-\underline{q}) + E_h(\underline{k}-\underline{q}) - \hbar\omega\,, \tag{B.8}$$

which is the same result obtained if instead we consider phonon absorption. Thus, the matrix elements for the processes resulting in indirect recombination are

$$|M|^2 = \left(\frac{e}{mc}\right)^2\left(\frac{2\pi c^2\hbar}{\varepsilon_\infty\omega}\right)\left(\frac{\hbar}{2\rho\Omega_o}\right)Q_o^2 n_o \frac{|P_{cv}(\underline{k}-\underline{q})|^2}{[E_\Gamma(\underline{k}-q) + E_h(\underline{k}-\underline{q}) - \hbar\omega]^2} \tag{B.9}$$

for phonon absorption and photon emission and

$$|M|^2 = \left(\frac{e}{mc}\right)^2\left(\frac{2\pi c^2 h}{\varepsilon_\infty\omega}\right)\left(\frac{h}{2\rho\Omega_o}\right)Q_o^2(n_o + 1) \frac{|P_{cv}(\underline{k}-\underline{q})|^2}{[E_\Gamma(\underline{k}-\underline{q}) + E_h(\underline{k}-\underline{q}) - h\omega]^2} \tag{B.10}$$

for photon and phonon emission, where $|P_{cv}(\underline{k}-\underline{q})|^2$ is given by Eq. (B.6).

The electron-phonon coupling constant used was $Q_o = 1.85 \times 10^{-3}$ erg/cm,[30] while the phonon energy was chosen as the average of the longitudinal optical and longitudinal acoustical L-point phonon energies.

REFERENCES

1. A. L. Smirl, PhD Dissertation, The University of Arizona, 1975.

2. J. C. Matter, PhD Dissertation, The University of Arizona, 1975.

3. D. H. Auston and C. V. Shank, Phys. Rev. Lett. 32, 1120, 1974.

4. A. Elci, M. O. Scully, A. L. Smirl, and J. C. Matter, Phys. Rev. B 16, 191, 1977.

5. A. L. Smirl, P. Latham, A. Elci, and J. S. Bessey, Internat. Conf. Hot Electrons, Denton, Tex., 1977.

6. S. Block and G. Piermarini, Physics Today 29(10), 44, 1976.

7. G. J. Piermarini and S. Block, Rev. Sci. Instr. 46, 973, 1975.

8. B. Welber, Rev. Sci. Instr. 47, 183, 1976.

9. A. L. Smirl, J. C. Matter, A. Elci, and M. O. Scully, Opt. Commun. 16, 118, 1976.

10. M. Cardona and W. Paul, J. Phys. Chem. Solids 17, 138, 1960.

11. W. Paul and D. M. Warschauer, J. Phys. Chem. Solids 5, 89, 1958.

12. A. L. Smirl, North Texas State University, personal communication, 1977.

13. C. V. Shank and D. H. Auston, Phys. Rev. Lett. 34, 479, 1975.

14. W. Hagan, Max-Planck-Institut, Stuttgart, personal communication, 1977.

15. W. P. Dumke, Phys. Rev. 127, 1559, 1962.

16. M. J. Adams and P. T. Landsberg, in Proceedings of the Ninth International Conference on the Physics of Semiconductors, Moscow (Leningrad, Akademiya Nauk, 1968), p. 619.

17. J. R. Haynes and H. B. Briggs, Phys. Rev. 86, 847, 1952; J. R. Haynes, Phys. Rev. 98, 1866, 1955.

18. R. Newman, Phys. Rev. 91, 1313, 1953.

19. J. R. Haynes and N. G. Nilsson in Proc. 7th Int. Conf. Physics of of Semiconductors, Paris, Vol. 4, Radiative Recombination in Semiconductors (Dunod, Paris, 1965), p. 21.

20. H. M. van Driel, A. Elci, J. S. Bessey, and M. O. Scully, Solid State Commun. 20, 837, 1976.

21. C. Kittel, Quantum Theory of Solids (New York, Wiley, 1963).

22. M. Neuberger, "Group IV Semiconducting Materials," in Handbook of Electronic Materials, Vol. 5 (New York, Plenum, 1971).

23. W. van Roosbroeck and W. Shockley, Phys. Rev. 94, 1558, 1954.

24. S. M. Ryvken, Photoelectric Effects in Semiconductors (New York, Consultants Bureau, 1964), Chap. VIII.

25. J. M. Ziman, Principles of the Theory of Solids, ed. 2 (Cambridge, Cambridge University Press, 1972), p. 142.

26. A. C. Beer, M. N. Chase, and P. F. Choquard, Helv. Phys. Acta 28, 529, 1955.

27. W. van Roosbroeck, Phys. Rev. 91, 282, 1953.

28. H. Y. Fan, M. L. Shepherd, and W. Spitzer in Proceedings of the Conference on Photoconductivity, Atlantic City (New York, Wiley, 1956).

29. H. M. van Driel, University of Toronto, personal communication, 1977.

30. H. J. G. Meyer, Phys. Rev. 112, 298, 1958; J. Phys. Chem. Solids 8, 264, 1959.